https://doi.org/10.5194/egusphere-2026-2307
Preprint. Discussion started: 8 May 2026

Monitoring Stratospheric Aerosols over Europe: A 16-Year CALIPSO Dataset Analysis (2007–2022)

Christina-Anna Papanikolaou[1], Nikolaos Papagiannopoulos[1], Michail Mytilinaios[1], Pilar Gumà-Claramunt[1], Benedetto De Rosa[1], Giuseppe D'Amico[1], Aldo Amodeo[1] and Lucia Mona[1]

1 Consiglio Nazionale Delle Ricerche, Istituto di Metodologie per l'Analisi Ambientale (CNR-IMAA), 85050, Tito Scalo, Potenza, Italy

Correspondence to: Nikolaos Papagiannopoulos (nikolaos.papagianopoulos@cnr.it)

Abstract. Stratospheric aerosols exert strong radiative and dynamical impacts due to their long residence times and efficient transport. Using CALIPSO Level 2 version 4.51 profiles, we develop a 16-year (2007–2022) climatology of stratospheric aerosol occurrence, vertical structure, subtype composition, and optical depth over Europe, analyzing nighttime overpasses across 12 subregions. The record captures the dominant influence of major volcanic eruptions (Okmok and Kasatochi 2008, Sarychev Peak 2009, Grímsvötn and Nabro 2011, Raikoke 2019) and pyrocumulonimbus-driven wildfire events (e.g., Western Canada 2007, Pacific Northwest Event (PNW) 2017, Siberia 2019–2022). These episodic injections drive strong interannual variability, with annual mean nighttime stratospheric aerosol optical depth (sAOD) ranging from 0.032 in 2007 to a peak of 0.067 in 2017. Vertical distributions broaden over time, with frequent detections reaching heights of 17–19 km and extreme cases up to ~29.8 km, especially following Raikoke's eruption and major Siberian fire seasons. Subtype analysis reveals sulfate dominance in northern regions and smoke-driven anomalies during major wildfire years, while southern regions show larger unclassified fractions. While no monotonic trend is found, analysis reveals a change-point after 2016, marking a transition to a higher-loading regime. These results highlight the strongly event-driven nature of European stratospheric aerosol variability and CALIPSO's key role in long term monitoring of volcanic and wildfire impacts on the lower stratosphere.

1 Introduction

Stratospheric aerosols play a critical role in Earth's radiation budget and atmospheric dynamics, with their prolonged residence time significantly influencing climate and weather patterns (e.g., Domeisen and Butler, 2020; Khaykin et al., 2020; Yu et al., 2021). These aerosols originate from a variety of sources, including volcanic eruptions and biomass-burning events, and they different chemical and radiative impacts (Tackett et al., 2023).

The injection of volcanic sulfur dioxide (SO_2) leads to the formation of sulfate aerosols that reside for 1-3 years in the stratosphere. These particles primarily scatter incoming solar radiation, resulting in a net negative radiative forcing at the top-of-the-atmosphere (TOA) and a consequent cooling at the surface (Aubry et al., 2021; Schallock et al., 2023). In contrast, volcanic ash particles are relatively large and sediment after some hours or days, generally resulting in only minor

https://doi.org/10.5194/egusphere-2026-2307
Preprint. Discussion started: 8 May 2026

climatic significance compared to the sulfate aerosols (Boucher, 2015; Schallock et al., 2023). The radiative impact of wildfire smoke differs significantly from these volcanic events due to the presence of light-absorbing carbonaceous particles. Injections from pyrocumulonimbus (pyroCb) events introduce smoke particles directly into the midlatitude stratosphere, where they can have a global impact on the radiation budget and stratospheric dynamics (Yu et al., 2021; Senf et al., 2023). Radiative heating of these absorbing smoke particles causes "self-lofting" and, in the case of extreme events such as the 2019-2020 Australian fires, the formation of synoptic-scale anticyclonic vortices that lift smoke-containing airmasses into the middle stratosphere (Kablick et al., 2020; Allen et al., 2020; Ma et al., 2024).

Cloud-Aerosol Lidar and Infrared Pathfinder Satellite Observation (CALIPSO)—a joint mission by NASA and CNES—has provided an unparalleled record of aerosol and cloud profiles from space. Its primary instrument, the Cloud-Aerosol Lidar with Orthogonal Polarization (CALIOP), operated at two wavelengths (532 nm and 1064 nm), offering vertically resolved measurements of aerosols and clouds from April 28, 2006, until its operational end on August 1, 2023 (Winker et al., 2009; Omar et al., 2009). Over its 17-year mission, CALIPSO has played a pivotal role in climatological studies by delivering a unique, continuous record of aerosol and cloud profiles from space. These data have been essential for evaluating and improving climate models, particularly in regions where ground-based observations are sparse (Winker et al., 2012; Papanikolaou et al., 2022). CALIPSO's observations have helped quantify aerosol radiative forcing, assess cloud phase and thickness, and monitor long-range transport of dust, smoke, and pollution—all of which are vital for understanding Earth's energy balance and climate feedback mechanisms (Proestakis et al., 2024). Additionally, its Level 3 climatological products have been validated against ground-based networks such as the EARLINET (European Aerosol Research Lidar Network; Pappalardo et al., 2014) enhancing confidence in satellite-derived datasets used in climate research (Papagiannopoulos et al., 2016; Thomason et al., 2018). Beyond its contributions to climatology, CALIPSO has proven especially valuable in advancing stratospheric studies thanks to its detection and classification of aerosol layers above the tropopause—including volcanic ash, sulfate aerosols, polar stratospheric aerosols (PSAs) and smoke from pyroCb (Kim et al., 2018; Ohneiser et al., 2021; Tackett et al., 2023). In 2023, the release of CALIPSO's Version 4.51 stratospheric aerosol subtyping algorithm marked a major advancement in data quality and interpretability (Tackett et al., 2023). This update introduced refined classification criteria, including a dedicated sulfate aerosol subtype and a new "unclassified" category for diffuse layers, enhancing the accuracy of aerosol identification. The algorithm also improved discrimination between volcanic ash and smoke, particularly in complex scenarios such as daytime pyroCb events. These enhancements not only sharpen our understanding of stratospheric aerosol behaviour but also reinforce CALIPSO's legacy as a vital tool for atmospheric and climate science.

In recent years, extreme wildfire patterns have become more prevalent across the North Hemisphere (NH), leading to notable changes in the composition and dynamics of stratospheric aerosols (Halofsky et al., 2020). Massive smoke injections from pyroCb clouds can now rival moderate volcanic eruptions in terms of optical depth and longevity, significantly impacting the stratospheric aerosol load and its subsequent climatic feedback (Hirsch and Koren, 2021). The European stratosphere serves as a critical receptor for the long-range transport of these plumes, particularly those originating from

https://doi.org/10.5194/egusphere-2026-2307
Preprint. Discussion started: 8 May 2026

intense wildfire activity in North America and Siberia. Additionally, it provides a framework for stratospheric studies using European research infrastructures and dedicated to stratosphere profiling research sites (e.g., Mattis et al., 2010; Pappalardo et al., 2014). EARLINET, part of the Aerosols, Clouds and Trace gases Reaserch Infrastructure (ACTRIS), ground-based observations have documented these events; for instance, the unprecedented 2017 Canadian wildfire smoke was extensively monitored, as it crossed the European continent, providing a unique opportunity to study the event (Ansmann et al., 2018; Haarig et al., 2018; Hu et al., 2019). Additionally, long-term monitoring at European sites, such as Garmisch-Partenkirchen, has further documented both volcanic and biomass-burning intrusions over several decades (Trickl and Giehl, 2013; Trickl et al., 2024).

In this study, we utilize the multiyear aerosol data record from the CALIPSO satellite to gain comprehensive insights into stratospheric aerosols over Europe. Specifically, we aim to document the occurrence and variability of different stratospheric aerosol types over a 16-year period (2007 to 2022). By systematically analyzing the temporal and spatial distribution of stratospheric aerosols over Europe, this study provides new insights into the long-term variability and sources of stratospheric aerosols. The findings of this study will contribute to a deeper understanding of the interactions between wildfire emissions, volcanic activity, and atmospheric processes, ultimately improving our ability to assess the climatic impact of stratospheric aerosols.

The paper is organized as follows. Section 2 describes the data and methodologies employed in this study. Section 3 presents the main results and discusses their broader implications and associated uncertainties. Finally, Section 4 provides a summary of the key conclusions.

2 Methodology

To evaluate the long-term evolution of stratospheric aerosols over Europe, we developed a data processing workflow based on the CALIPSO Version 4.51 products. The methodology is implemented in three stages: first, we define the study region and keep the more accurate, due to high signal-to-noise ratio nighttime data; next, we apply standard quality-assurance criteria to the Level 2 parameters to ensure retrieval integrity and a statistical artifact removal method; and finally, we perform a data analysis involving yearly, seasonal and regional averaging.

2.1. CALIPSO Products & Study Region

In this study we use the CALIPSO Level 2 (L2) version 4.51 Aerosol Profile (APro), which incorporates significant advancements with respect to its predecessor as detailed in Tackett et al. (2023). The L2 APro is provided at a horizontal resolution of 5 km, along with the Vertical Feature Mask (VFM;Kim et al., 2018; Winker et al., 2009). The primary aerosol optical properties used in this study include the aerosol backscatter coefficient (b_{aer}) and aerosol extinction coefficient (a_{aer}) at 532 nm, and the stratospheric aerosol optical depth (sAOD), derived by integrating each a_{aer} profile over the stratospheric aerosol load. As an elastic lidar, CALIOP retrieves aerosol extinction using predefined lidar ratio values assigned to each aerosol subtype, derived from empirical measurements, modeling, and a multi-year Aerosol Robotic Network (AERONET)

https://doi.org/10.5194/egusphere-2026-2307
Preprint. Discussion started: 8 May 2026

dataset (Young et al., 2018). The uncertainty in lidar ratio values is estimated at approximately 30%, potentially leading to over- and underestimations of aerosol extinction, particularly in low-aerosol-concentration regions (Ansmann et al., 2021a).

The study region was defined between 35°N and 65°N and from 10°W to 30°E, covering a broad area over the European continent. This domain was further subdivided into 12 study zones of 10°×10° (Figure 1). Within each zone, CALIPSO-derived aerosol data were spatially averaged, and analyzed for each satellite overpass to assess temporal and regional variability in stratospheric aerosol loading. To ease readability, each subregion was named after the following convention, based on latitude and longitude ranges: N for Northern Europe (55° – 65°N), C for Central Europe (45° – 55°N), and S for Southern Europe (35° – 45°N). The longitudinal regions are denoted numerically: 1 for 10°W – 0°, 2 for 0° – 10°E, 3 for 10° – 20°E, and 4 for 20° – 30°E.

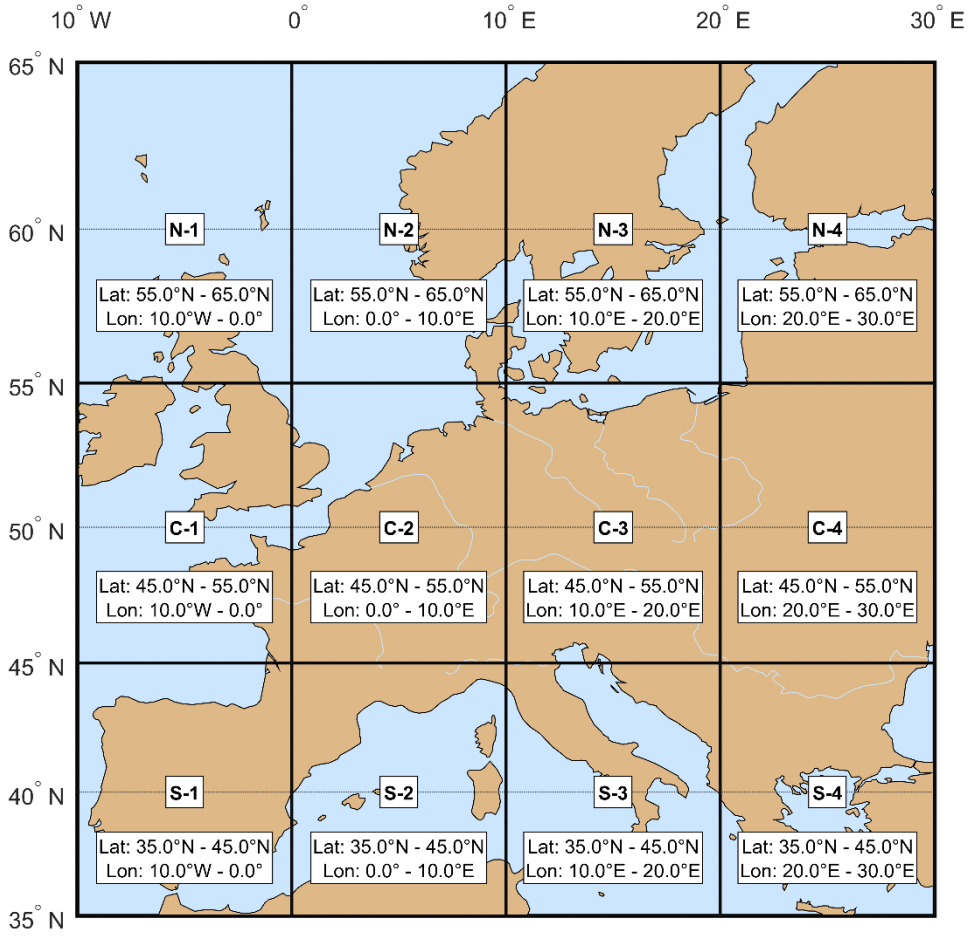

Figure 1: Region and subregions used in this study. For the latitudinal divisions (letters), N stands for north, C for central, and S for south. For the longitudinal divisions, 1 refers to 10°W – 0°, 2 to 0° – 10°E, 3 to 10° – 20°E, and 4 to 20° – 30°E. This 12-subregion grid and labeling convention are maintained in all relative subsequent figures.

https://doi.org/10.5194/egusphere-2026-2307
Preprint. Discussion started: 8 May 2026

2.2 Quality-assurance criteria and classification

The APro dataset was processed by applying quality-assurance criteria beyond the standard CALIPSO products (https://www-calipso.larc.nasa.gov/resources/calipso_users_guide/data_desc/cal_lid_l2_profile_v4-51_desc.php; last access: 15 March 2026). Due to the lower signal-to-noise ratio (SNR) at high altitudes, the Cloud-Aerosol Discrimination (CAD) algorithm may have reduced performance, resulting in lower absolute CAD scores. CAD scores range within −100 and 100. A positive score indicates a cloud, while a negative score indicates an aerosol. The absolute value of the score represents the algorithm's confidence level (100 being the highest). In our analysis, we retained only layers with CAD scores between −100 and −20. By setting the lower bound at −20, we exclude features with low-confidence classifications (scores between 0 and −20) from clouds or polar stratospheric clouds (PSCs) (Kar et al., 2019). The extinction QC flag summarizes the final state of the retrieval; specifically, we accepted only high-confidence samples (values 0, 1, 16, and 18) representing successful constrained or unconstrained solutions where the initial lidar ratio was either unchanged or correctly adjusted. Furthermore, we rejected all layers with an extinction uncertainty equal to 99.99 km^{-1}, as this value identifies algorithmic divergence (Tackett et al., 2018).

The VFM data product (https://www-calipso.larc.nasa.gov/resources/calipso_users_guide/data_desc/cal_lid_l2_vfm_v4-51_desc.php; last access: 15 March 2026) describes the vertical and horizontal distribution of cloud and aerosol layers observed by CALIOP. For each layer detected in the profile, a set of feature classification flags is derived. These flags report on: (a) feature type (e.g., cloud vs. tropospheric aerosol vs. stratospheric aerosol); (b) feature subtype; (c) layer ice-water phase (clouds only); and (d) the amount of horizontal averaging required for layer detection. Only stratospheric aerosol profiles and their corresponding subtypes: smoke (type 6), polar stratospheric aerosols (type 8), volcanic ash (type 9), sulfate aerosols (type 10), and unclassified aerosols (type 11) were considered. Despite advancements in the stratospheric aerosol subtyping algorithm and lidar ratio assignments in the Version 4.5 Level 2 dataset, some uncertainties remain. In particular, smoke transported from the troposphere into the Upper Troposphere and Lower Stratosphere (UTLS) via self-lofting, rather than direct pyroCb activity, may still be misclassified as sulfate due to the similarly low depolarization values of both aerosol types (Tackett et al., 2023).

To ensure a reliable analysis, we restricted our dataset to nighttime observations only (Kar et al., 2019; Tackett et al., 2018). This approach takes advantage of the optimized SNR found in the absence of solar interference. This is important for the accurate detection of thin and faint stratospheric aerosol layers, which are often lost or hidden by background noise during daytime orbits (Winker et al., 2012). Lower SNR also contributes to higher uncertainty in the daytime level 2 extinction retrievals (Young et al., 2018; Tackett et al., 2018). Because solar background signals degrade the daytime SNR and make accurate layer (and surface) detection more difficult, nighttime retrievals are considered to be of higher quality than daytime retrievals, to be more accurate although it is possible that the lidar ratio is still too high in both cases.

https://doi.org/10.5194/egusphere-2026-2307
Preprint. Discussion started: 8 May 2026

2.3 Outliers removal

During data processing, certain artifacts that persisted despite the applied filtering procedures were identified, occasionally influencing the results. An example of such an artifact is illustrated in Fig. 2.

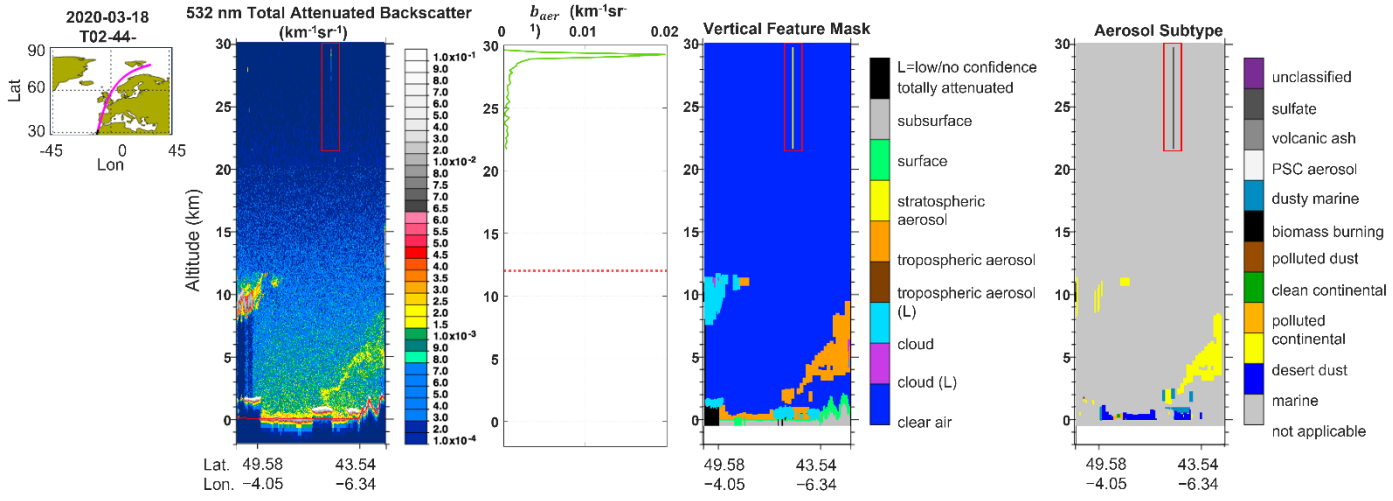

Figure 2: Example of CALIPSO a hot pixel observed in the stratosphere on 18 March 2020 at 02:44:17 close to 30 km altitude in (from left to right) the 532 nm total attenuated backscatter, the 532 nm aerosol backscatter coefficient, the vertical feature mask, and the aerosol subtype classification. The artifact is highlighted with a red rectangle.

In this specific scene, it was observed that a highly attenuating red (hot) pixel was misclassified as sulfate. Such cases, characterized by anomalously high backscatter coefficients, lead to spikes that are significantly elevated compared to typical stratospheric aerosol backscatter values and, also, do not physically resemble aerosol features. Therefore, a procedure that accounts for the identification of these artifacts and their removal was devised.

To address this issue and eliminate these non-physical backscatter "spikes" in such a big dataset, we performed a distribution-based filtering of the 532 nm b_{aer}. This process was applied across the entire vertical extent of each nighttime stratospheric profile. The filtering threshold was determined by calculating the Probability Density Function (PDF) for the complete nighttime dataset (Fig. 3). The grey shaded areas indicate the percentage of data points falling within 1σ, 2σ, and 3σ. The red dotted line illustrates the mean (μ), and the black dashed line the μ+3σ.

https://doi.org/10.5194/egusphere-2026-2307
Preprint. Discussion started: 8 May 2026

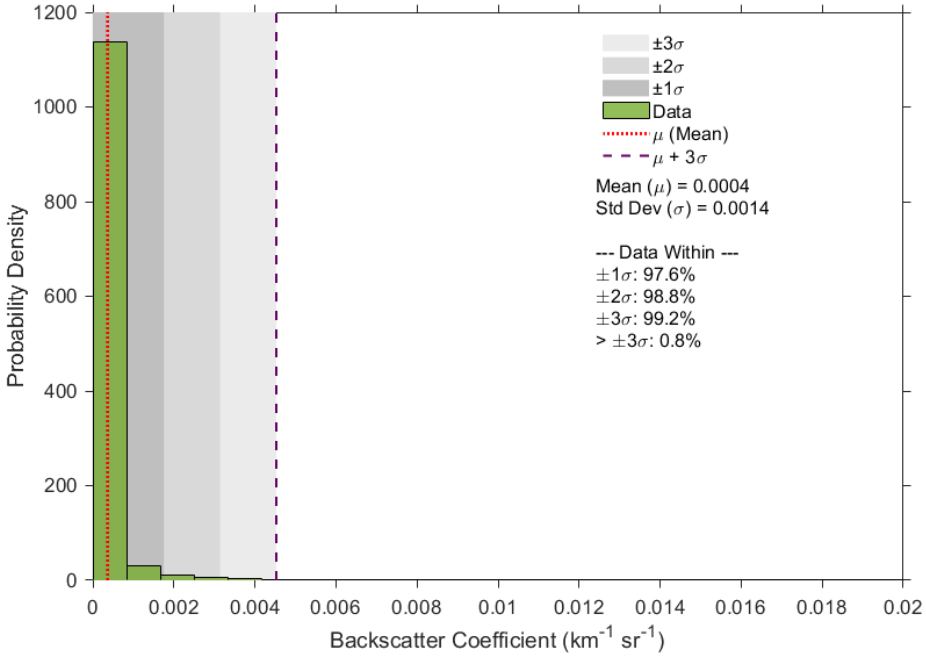

Figure 3: Probability density of backscatter coefficient values at 532 nm, observed throughout the years 2007-2022 in all sub-regions.

The clipping threshold was established at 0.005 $km^{-1}sr^{-1}$, corresponding to the μ+3σ of the distribution. Based on this criterion, 1,063 data points (0.8% of the total dataset) were identified as artifacts and discarded. The impact of this refinement is evident in the shift of the dataset's central tendency: the initial mean of 0.0004 $km^{-1}sr^{-1}$ was reduced to a clipped mean of 0.0003 $km^{-1}sr^{-1}$, providing a more robust baseline for the subsequent sAOD calculations.

2.4 Spatio-Temporal analysis

Following the quality control provided in Sect 2.2-2.3, the high-resolution data were averaged both temporally and spatially to generate a comprehensive European stratospheric climatology. This process involved the synthesis of the stratospheric aerosol optical depth (sAOD) and the identified aerosol subtypes across multiple scales of analysis. Initially, the data were spatially averaged within each of the 12 predefined 10°×10° study zones to assess localized variations and regional transport pathways. To ensure that seasonal analyses align strictly within a single calendar year and to avoid the overlap inherent in the conventional DJF (December-January-February) winter definition, we defined winter by treating January and February separately from December of the same year. This adjustment allows for a clearer representation of interannual variations, while the definitions for the remaining seasons—spring, summer, and autumn—follow the standard calendar months. To characterize the overall stratospheric state, we computed both yearly averages and seasonal contributions for each sub-region, alongside a pan-European assessment representing the whole study area. This integrated approach allows for the quantification of the total aerosol load while simultaneously evaluating the relative dominance of specific species, such as

https://doi.org/10.5194/egusphere-2026-2307
Preprint. Discussion started: 8 May 2026

smoke, sulfate, or volcanic ash, within the different regions and years. By synthesizing these regional and temporal averages, we provide a robust framework to characterize the long-term evolution and the shifting compositional state of the European stratospheric aerosol layer throughout the 16-year study period.

3 Results and Discussion

3.1 Events occurred during the 16-year study period

Both explosive volcanic eruptions and large-scale wildfire events are major contributors of aerosol loading in the stratosphere. During the 16-year period from 2007 to 2022, several significant natural events with the potential to influence the composition and amount of the stratospheric aerosol load over Europe were observed.

Table 1 lists significant explosive volcanic eruptions that occurred in the NH between 2007 and 2022, potentially influencing the stratospheric aerosol load over Europe during the study period. The size of these explosive events is characterized using the Volcanic Explosivity Index (VEI), a widely adopted semi-quantitative scale developed by Newhall and Self (1982). VEI provides an estimate of eruption magnitude based primarily on the volume of ejected tephra and secondarily on the eruption column height, along with qualitative descriptors. The scale ranges from 0 to 8, where, for values greater than 2, every step corresponds to a tenfold increase in the bulk volume of eruptive material. Eruptions with VEI 4 or greater are generally considered capable of injecting significant amounts of volcanic gases (like SO_2) and ash directly into the stratosphere, leading to the formation of widespread aerosol layers with potential climatic and atmospheric chemistry impacts. Information and classifications for these eruptions are maintained by the Smithsonian Institution's Global Volcanism Program (GVP; https://volcano.si.edu, last access: 5 May 2025).

Table 1. List of the most significant Northern Hemisphere volcanic eruptions between 2007 and 2022 in terms of the parameter VEI (Volcanic Explositivity Index). Includes eruption date, volcano name, location, and VEI (VEI ≥ 3).

Eruption Date	Volcano Name	Location	VEI	References
12 Jul 2008	Okmok	Aleutian Islands, Alaska (53.4° N, 168.1° W)	4	(Schmale et al., 2010)
7 Aug 2008	Kasatochi	Aleutian Islands, Alaska (52.2° N,175.5° W)	4	(Di Pierro et al., 2013; Zerefos et al., 2017; Kristiansen et al., 2010; Hoffmann et al., 2010; Schmale et al., 2010)
15 Mar – 4 Apr 2009	Redoubt	Alaska (60.485°N, 152.742°W)	3	(Trickl and Giehl, 2013; Bull and Buurman, 2013)
11–16 Jun 2009	Sarychev Peak	Kuril Islands, Russia (48.1° N, 153.2° E)	4	(Di Pierro et al., 2013)

https://doi.org/10.5194/egusphere-2026-2307
Preprint. Discussion started: 8 May 2026

21 May 2011	Grímsvötn	Iceland (64.4° N, 17.3° W)	4	(Ansmann et al., 2012; Tesche et al., 2012; Prata et al., 2017)
13 Jun 2011	Nabro	Eritrea (13.4° N, 41.7° E)	4	(Clarisse et al., 2014; Min et al., 2017; Aubry et al., 2021; Zerefos et al., 2017)
21-22 Jun 2019	Raikoke	Kuril Islands, Russia (48.3° N, 153.3° E)	4	(Ansmann et al., 2021a; Trickl et al., 2024; Voudouri et al., 2023; Ohneiser et al., 2021; Khaykin et al., 2022; Kloss et al., 2020; Vaughan et al., 2021; Grebennikov et al., 2020)
9 Apr 2021	La Soufrière	St. Vincent (13.3° N, 61.2° W)	4	(Taylor et al., 2023; Bruckert et al., 2023)

The eruptions summarized in Table 1 encompass events predominantly rated with VEI 3 or 4. These include high-latitude eruptions from the Aleutians and Alaska, like Okmok (Schmale et al., 2010) and Kasatochi in 2008 (Zerefos et al., 2017), the Redoubt eruption in 2009 (Bull and Buurman, 2013), and the Sarychev Peak eruption in 2009, in Kuril Islands in Russia (Di Pierro et al., 2013) and the Grímsvötn in 2011 (Prata et al., 2017), and Raikoke in 2019 (Voudouri et al., 2023), as well as tropical or subtropical eruptions like Nabro in 2011 (Aubry et al., 2021) and La Soufrière in 2021 (Bruckert et al., 2023). These specific explosive events highlight the perturbation of the stratosphere during the analysis timeframe.

It is worth noting that while tropical eruptions in the Southern Hemisphere (SH), such as Mt. Kelud in 2014 and Hunga Tonga eruption in 2022 likely contributed to the global stratospheric aerosol background, they are not featured in Table 1. This study prioritizes events where the transport pathways and aerosol optical signatures were most clearly distinguishable at European latitudes. By focusing on these specific sources, we maintain a high degree of confidence in the attribution of observed stratospheric perturbations to their respective volcanic origins.

Unlike volcanic eruptions, there is no equivalent standardized index to quantify the stratospheric injection potential of wildfires. Instead, the assessment of a wildfire's impact on the stratosphere relies on post-event analysis of several factors. The most critical indicator is the pyroCb cloud formation reaching or exceeding the tropopause height, as these fire-driven thunderstorms provide a direct pathway for injecting large quantities of smoke aerosols and gases into the lower stratosphere (Torres et al., 2020; Yu et al., 2021; Fromm et al., 2019; Tencé et al., 2022; Christian et al., 2019; Peterson et al., 2018b; Kablick et al., 2020). Complementary evidence includes satellite measurements of plume altitude, enhancements in sAOD, estimated smoke mass injected, and the observed persistence and transport range of the resulting stratospheric smoke layers. Table 2 summarizes major wildfire events in the NH between 2007 and 2022, based on documented PyroCb activity or subsequent widespread stratospheric smoke observations, to have likely contributed significantly to the stratospheric aerosol load during the study period. This list focuses on large-scale events with recognized stratospheric consequences potentially observable over Europe and may not be exhaustive of all pyroCb occurrences globally.

https://doi.org/10.5194/egusphere-2026-2307
Preprint. Discussion started: 8 May 2026

Table 2. Summary of major Northern Hemisphere wildfire periods (2007-2022) known for producing pyroCb clouds and potentially injecting significant smoke aerosols into the stratosphere.

Event Name/Region	Period	Reference
Western Canada Fires	May & Jul-Aug 2007	unavailable
Siberian Fires	May-Jun 2012	unavailable
Canadian Wildfires (PNW Event)	Aug 2017	(Ansmann et al., 2018; Das et al., 2021; Torres et al., 2020; Peterson et al., 2018a; Baars et al., 2019; Haarig et al., 2018; Hu et al., 2019)
Siberian Wildfires	Summer 2019	(Ansmann et al., 2021a, 2022)
US West Coast Wildfires	Aug-Sep 2020	(Ansmann et al., 2021b; Baars et al., 2021; Mamouri et al., 2023)
Canadian Wildfires	Summer 2021	(Sharma et al., 2024)
Siberian Wildfires	Summer 2021	(Popovicheva et al., 2025; Cheremisin et al., 2022)
Siberian Wildfires	May-Summer 2022	(Popovicheva et al., 2025)

The wildfire events listed in Table 2 represent some of the most significant episodes that influenced the stratospheric aerosol budget through the years. PyroCb activity acts as the primary conduit for lofting biomass burning aerosols to altitudes where their atmospheric lifetime is significantly extended, allowing for long-range transport (Fromm, 2010). The 2017 Pacific Northwest Event (PNW) originating in British Columbia, Canada, was particularly impactful, injecting an estimated 0.1-0.3 Tg of smoke via multiple intense pyroCbs (Ansmann et al., 2018; Das et al., 2021; Torres et al., 2020; Peterson et al., 2018a; Baars et al., 2019; Haarig et al., 2018; Hu et al., 2019). This resulted in dense stratospheric smoke layers observed over Europe and widely across the NH, for several months afterwards. Large Siberian wildfires, notably during the summer of 2019 (Ansmann et al., 2021a), were also identified as substantial sources contributing to stratospheric smoke observed over Europe (Ansmann et al., 2021a, 2022), co-existing with volcanic aerosols from the Raikoke eruption that year (Voudouri et al., 2023). Furthermore, intense US West Coast fires in 2020 (Ansmann et al., 2021b; Baars et al., 2021; Mamouri et al., 2023) and significant fire seasons with pyroCb activity in Canada and Siberia in 2021 and 2022 (Sharma et al., 2024; Popovicheva et al., 2025), contributed notable amounts of smoke to the UTLS.

3.2 Stratospheric aerosol observations and vertical distribution

https://doi.org/10.5194/egusphere-2026-2307
Preprint. Discussion started: 8 May 2026

Figure 4 presents the total number of nighttime aerosol profiles – defined as the orbital average of aerosol profiles per subregion together with the number of profiles containing stratospheric aerosols.

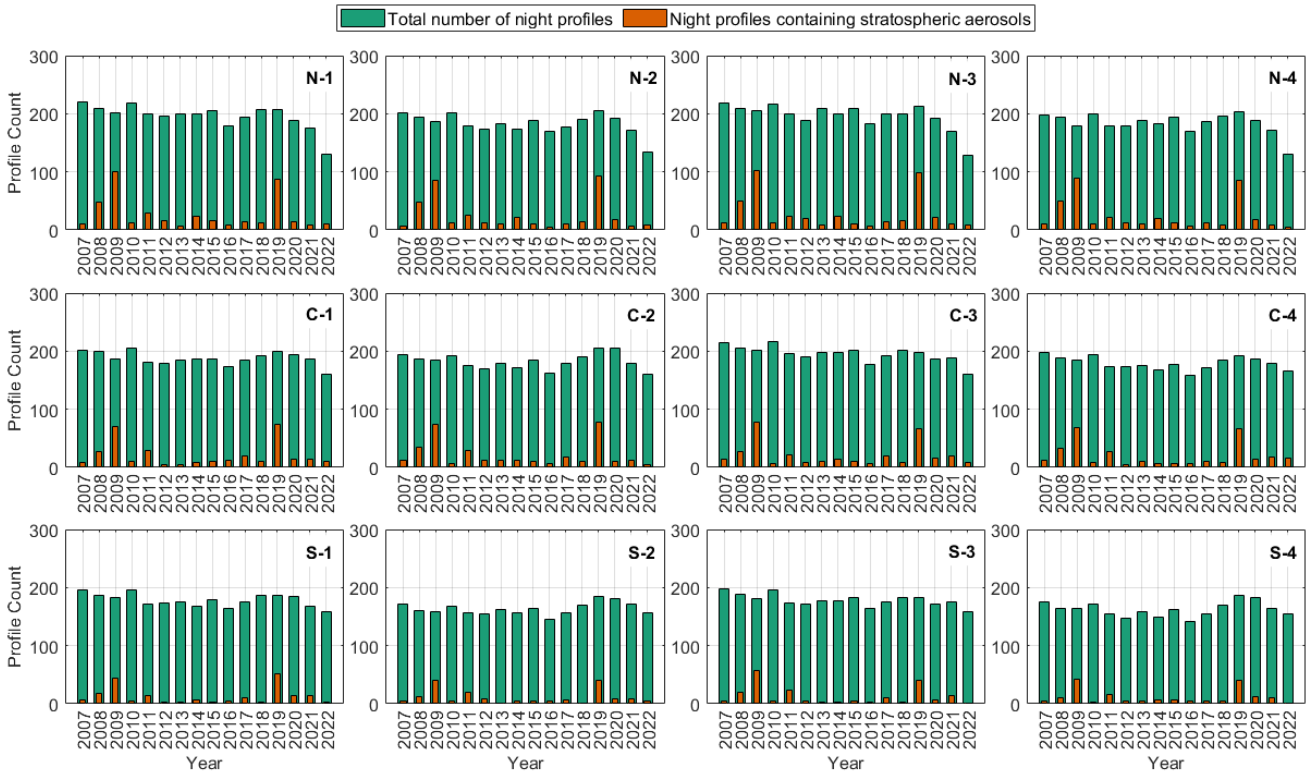

Figure 4: Graph bars showing the total number of nighttime aerosol profiles (green) and number of profiles containing stratospheric aerosols (orange).

CALIOP stratospheric observations across Europe show distinct spatial and temporal variations. The most pronounced peaks occurred in 2009 and 2019, with nearly all subregions—particularly those in the north (N-1 through N-4)—registering their highest counts of valid nighttime stratospheric profiles in those years. For instance, N-3 and N-2 reached 103 and 86 stratospheric profiles respectively in 2009, with similarly elevated numbers in 2019. Southern regions (S-1 to S-4) consistently showed lower overall number of stratospheric profiles, though they mirrored the same peak years, particularly S-1 and S-3 which saw moderate increases (44 and 57 respectively) in 2009. In contrast, 2016 and 2022 marked wide low points, with most regions—north, central, and south—reporting fewer than 10 stratospheric profiles in many instances. Central Europe (C-1 to C-4) generally had intermediate values, peaking modestly in 2009 and 2019. Longitudinally, eastern subregions (e.g., N-4, C-4, S-4) maintained slightly lower values compared to their western counterparts in several peak years.

Figure 5 illustrates the vertical distribution of stratospheric aerosols across the 12 European subregions from 2007 to 2022.

https://doi.org/10.5194/egusphere-2026-2307
Preprint. Discussion started: 8 May 2026

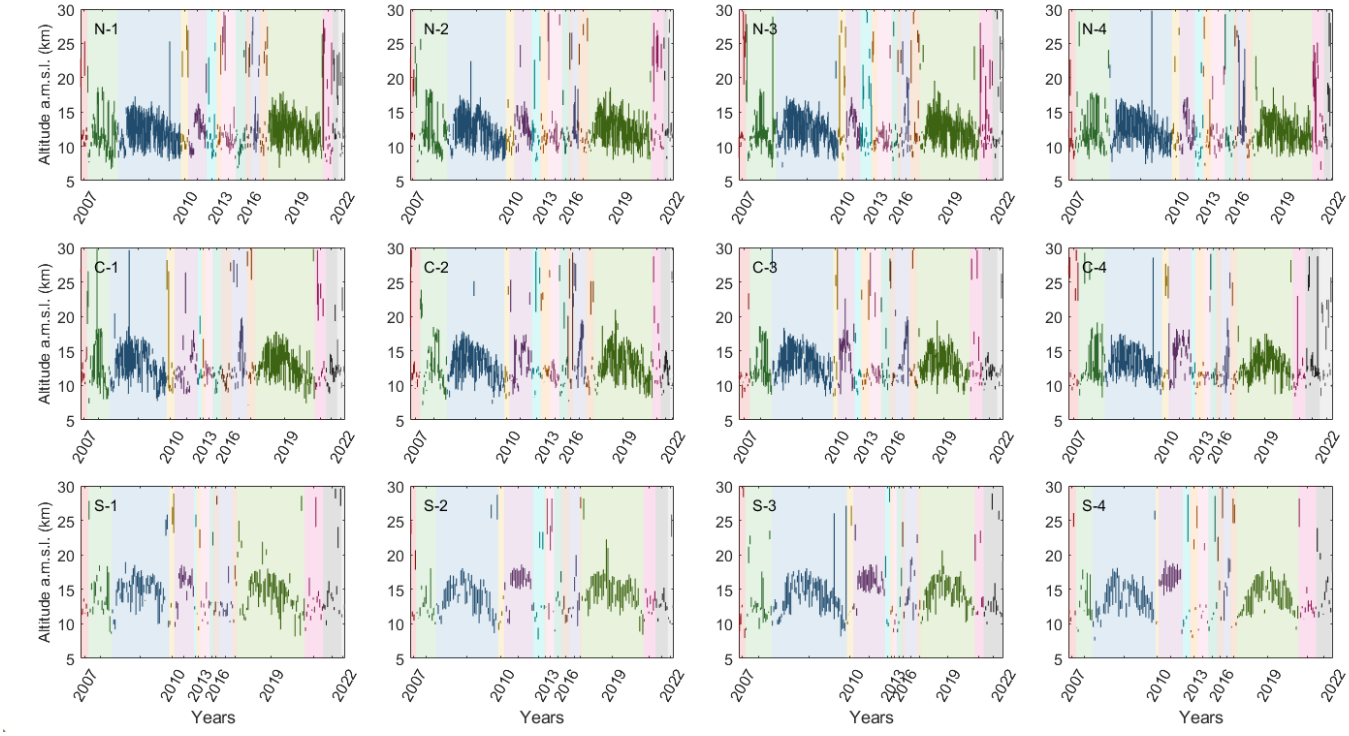

Figure 5: Vertical distribution of stratospheric aerosols across the 12 subregions. The different background and line colors denote the different years. Varying width of the corresponding-colored area indicates the number of observations per year.

While stratospheric aerosol layers are consistently observed across all regions, the data show a progressive increase in the vertical extent and altitude that aerosols reach, with the most elevated distributions occurring in 2022 and the latter years of the study. This trend is largely driven by the increasing frequency of pyroCb events and intense wildfire seasons, which injected smoke plumes deep into the stratosphere. In the Northern regions, N-1 layers shifted from a range of 10.10–13.86 km in 2009 (following the Sarychev Peak eruption) to a significantly higher 12.07–14.53 km in 2022. N-2 moved from a low and narrow range of 10.82–11.74 km in 2013 to a wider 12.67–15.14 km in 2022. N-3 exhibited broad extents early on (14.82–16.99 km in 2007) and reached its highest average top of 17.82 km in 2022. N-4 displayed high vertical extents during the 2009 volcanic period (10.50–14.18 km) and remained elevated in 2021 (13.67–16.04 km) following the La Soufrière and Siberian fire events.

The Central regions also varied significantly. C-1 was dynamic, moving from a narrow range of 10.92–11.54 km in 2015 to a wide 13.61–15.37 km in 2020. C-2 contrasted a narrow 10.82–11.92 km in 2014 with an upward expansion to 13.40–13.85 km in 2022, having also peaked significantly in 2017 (14.66–17.16 km) due to the Canadian PNW wildfires. C-3 showed broad distributions in 2009 (11.75–14.88 km) and 2011 (13.14–15.65 km) and continued this trend with 12.55–13.49 km in 2022. C-4 experienced a dramatic shift from very narrow ranges in 2012/2013 (around 11 km) to a much wider 13.92–15.41 km by 2022, directly reflecting the impact of Siberian smoke transport into Eastern Europe.

https://doi.org/10.5194/egusphere-2026-2307
Preprint. Discussion started: 8 May 2026

Across Southern Europe, S-1 varied from 11.77–12.29 km in 2007 to a broader 13.71–16.06 km in 2019 following the Raikoke eruption. S-2 demonstrated extreme variations, moving from a narrow 11.07–12.23 km in 2016 to an anomalous peak of 26.74–28.36 km in 2018, before settling at 13.90–15.02 km in 2022. S-3 showed broad extents in 2007 (13.53–14.88 km), narrowed significantly in 2014 (9.92–10.50 km), and returned to a higher 15.25–19.08 km in 2022. Finally, S-4 displayed a general upward shift, expanding from 10.10 km in 2010 to 17.58 km in 2022.

3.3 Stratospheric aerosol types and sAOD regional annual analysis

Figure 6 illustrates the long-term (2007–2022) spatial distribution of the averaged stratospheric aerosol loading and composition across Europe. It presents the aerosol subtype percentages along with 16-year mean classified profile counts for the 12 European subregions (N1-S4) nighttime CALIPSO observations.

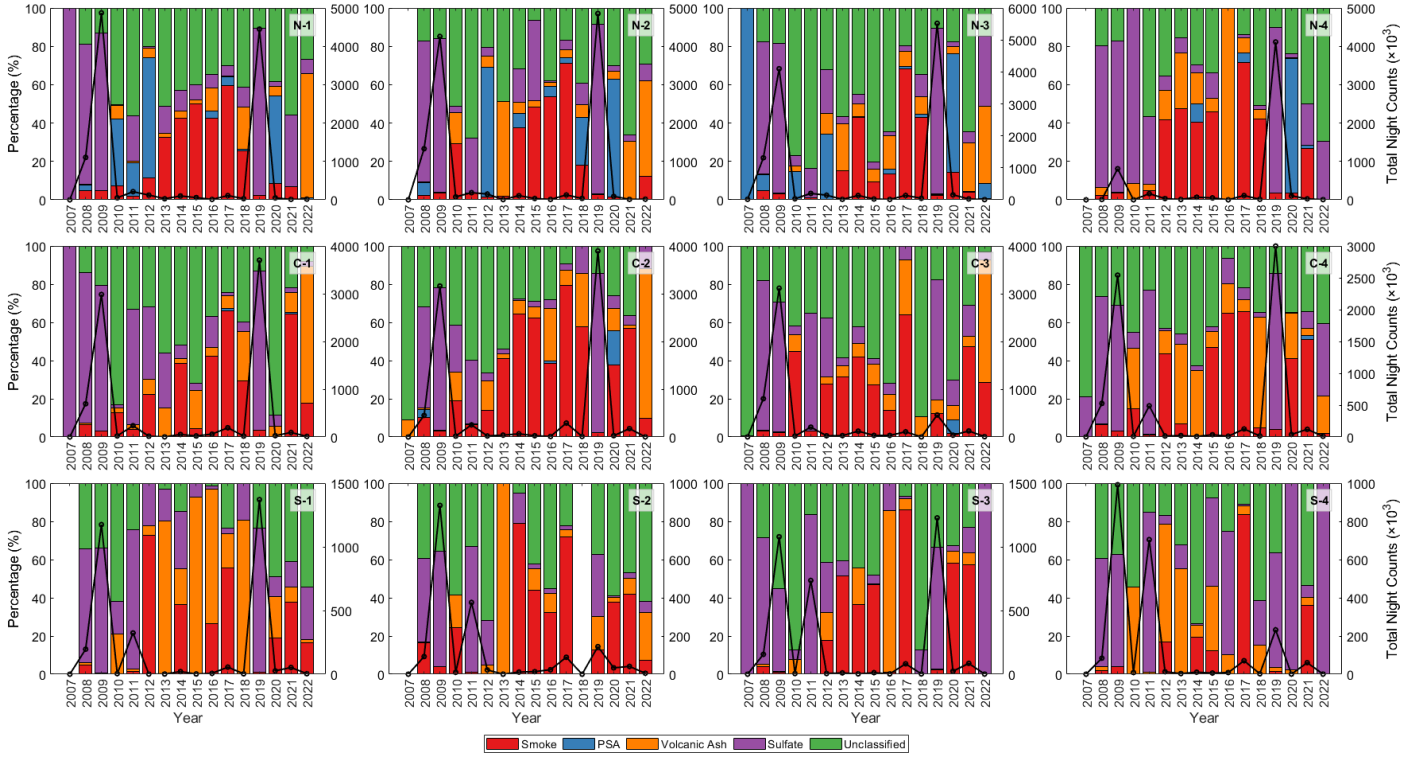

Figure 6: Time series (2007–2022) of annual CALIPSO profile counts in the stratosphere (black lines), attributed to different stratospheric aerosol subtypes—Smoke, PSA, Volcanic Ash, Sulfate, and Unclassified—and their percentage contribution to the total number of classified profiles (stacked bars), shown separately for each of the 12 European subregions.

nighttime observations yield high total counts (regional means up to ~1.2×10^7). The significant difference between day and night counts (1.6×10^6 and 6.7×10^6, respectively) in general, reflects the increased nighttime sensitivity of CALIOP. This is critical for the robust retrieval of thin stratospheric aerosol profiles, which are frequently attenuated or obscured by solar noise during daytime orbits. A distinct latitudinal gradient in counts (N>C>S) is evident, reflecting both CALIPSO's higher

https://doi.org/10.5194/egusphere-2026-2307
Preprint. Discussion started: 8 May 2026

285 sampling frequency poleward and likely the frequent impact on northern latitudes from the high-latitude NH sources. Depending on the strength of the Brewer–Dobson circulation, stratospheric materials such as aerosols can be rapidly transported from the tropics to high latitudes (Bègue et al., 2017).

More specifically, N1-N4 demonstrate the impact of the abovementioned events as well as seasonal Arctic processes. The persistent PSA fraction (~1.5–2.5%) is directly linked to winter low temperatures. The high background and volcanically
290 enhanced sulfate levels (~75–78%) reflect the cumulative SO_2 input from nearly all listed NH eruptions, both high-latitude and tropical (Nabro 2011, La Soufrière 2021), which most likely dispersed poleward due to the Brewer–Dobson circulation (Kloss et al., 2022; Fu et al., 2020). The notable smoke fraction (~4%–6%) integrates signals from Boreal forests fires seasons impacting the stratosphere. The moderate volcanic ash average (~1%) represents the blending of quiescent years with strong injections from eruptions like Kasatochi (2008) or Raikoke (2019).

295 A notable latitudinal gradient emerges at night; while the N regions are dominated by sulfate (~75–78%), the S regions exhibit a significant increase in the unclassified fraction (~28–36%). This gradient likely reflects the transition from relatively fresh, concentrated plumes to more “aged” or “mixed” aerosols in the South. Such low-intensity layers potentially lack the distinct optical signatures required for specific classification, leading to a higher frequency of unclassified detections as the aerosols disperse and evolve during their transport.

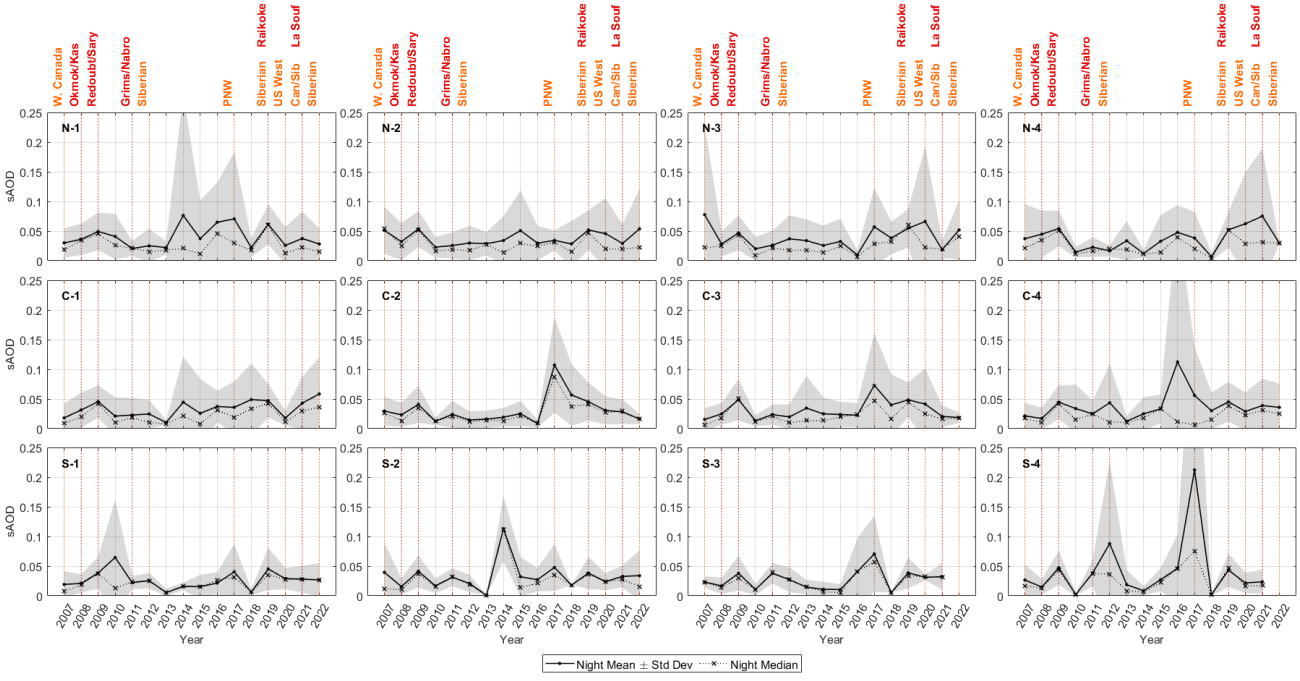

300

Figure 7: Time series (2007–2022) of the annual sAOD mean (continous black line) and median (dotted black line) during nighttime observations, for each of the 12 European subregions. Shaded areas correspond to the standard deviation (std).

https://doi.org/10.5194/egusphere-2026-2307
Preprint. Discussion started: 8 May 2026

Figure 7 displays the annual evolution of mean and median sAOD from 2007 to 2022 for each of the twelve European subregions. The plots show nighttime sAOD observations, with shaded areas representing the standard deviation (std). Across the study period, the time series revealed distinct annual fluctuations.

Combining Fig. 7 and Table 1 and 2, we observe the influence of the events on sAOD. The impact of high-latitude volcanic activity is particularly evident in the northern regions. The 2008 Okmok (53.4° N, 168.1° W; VEI 4) and Kasatochi (52.2° N, 175.5° W; VEI 4) eruptions, both originating from the Aleutian Islands, demonstrably left a clear signal, especially pronounced in the northernmost regions of our study (N-1, N-2, N-3). In Region N-1, the nighttime sAOD increased from 0.030±0.025 in 2007 to a peak of 0.049±0.032 in 2009. Similarly, N-2 maintained elevated nocturnal values, such as 0.054± 0.031 in 2009 and 0.052±0.033 in 2019. Despite high variability in certain years (e.g., N-1 in 2014), their persistence points to a sustained presence of stratospheric aerosols during nocturnal observations. This regional enhancement is directly attributable to the geographical proximity of these eruptions to the northern study areas, facilitating efficient transport and injection of aerosols.

Further contributing to the elevated sAOD levels in the subsequent year was the 2009 Sarychev Peak eruption (48.1° N, 153.2° E, VEI 4) in the Kuril Islands. This event's influence was particularly noticeable in 2009, with sAOD in N-2 at 0.054±0.031. The continued proximity of this eruption to the northern regions reinforces the observed localized impact.

Beyond these initial events, other significant injections played a role. A particularly strong sAOD signal is observed possibly following the 2011 Grímsvötn (64.4° N, 17.3° W, VEI 4) and Nabro (13.4° N, 41.7° E, VEI 4) eruptions. While Grímsvötn's higher latitude location affected the NH (Tesche et al., 2012; Zuev et al., 2017), Nabro's tropical injection allowed for wider global dispersion due to the Brewer-Dobson circulation (Sawamura et al., 2012). Elevated sAOD values were observed in 2014, particularly in the Central and Southern regions (e.g., C-1 sAOD: 0.045±0.077, S-2 sAOD: 0.113±0.055), even without a specific volcanic event present. The widespread Siberian and Canadian wildfires throughout the study period, particularly those listed in Table 2, would also have contributed to regional and potentially wider stratospheric aerosol burdens, especially in the northern latitudes where these events are more frequent.

Across the entire study period, the N regions consistently display the highest sAOD values and the largest fluctuations, particularly in years following major high-latitude volcanic eruptions (e.g., Okmok, Kasatochi, Grímsvötn) and significant wildfire seasons (e.g., Siberia, Canada). This is expected as these regions are often closer to the source of the injections and within the predominant transport pathways of stratospheric aerosols in the NH. It is worth noting that while tropical eruptions (e.g., Nabro) can have a more widespread, global impact on stratospheric aerosols due to atmospheric circulation patterns, their signature might be less intensely confined to specific regions compared to high-latitude events (Toohey et al., 2025).

3.4 Stratospheric aerosol types and sAOD regional seasonal contributions

The seasonal distribution of sAOD across the study period exhibits notable inter-annual variability. The averaged seasonal contributions to sAOD across all analyzed regions for nighttime conditions are presented in Fig. 8.

https://doi.org/10.5194/egusphere-2026-2307
Preprint. Discussion started: 8 May 2026

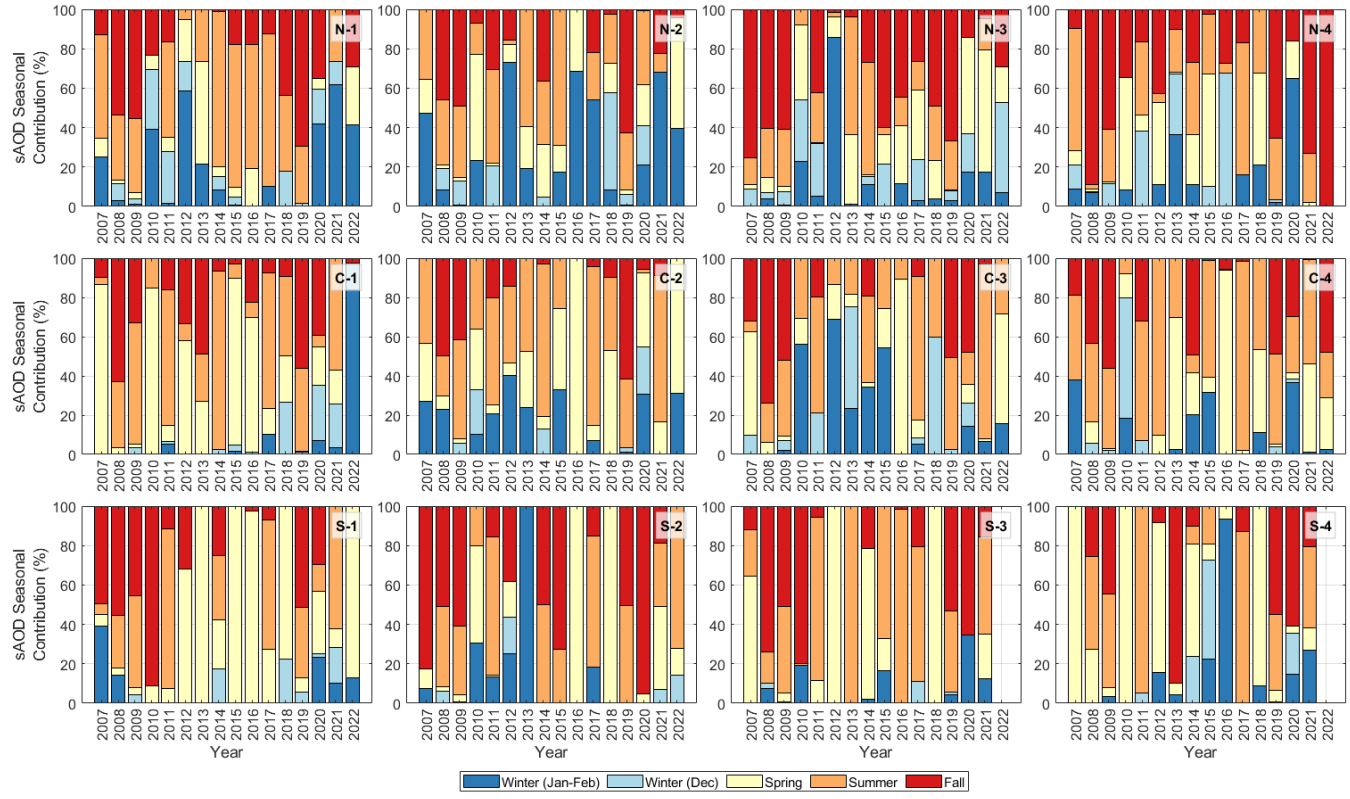

Figure 8: Seasonal percentage contribution to the nighttime sAOD, across the 12 European subregions. The seasons are defined as follows: Winter (split into Jan-Feb and Dec), Spring, Summer, and Fall, for the years 2007–2022.

Nighttime sAOD distributions exhibit strong seasonal variability, with the dominance of specific seasons shifting significantly according to regional proximity to aerosol sources and large-scale transport pathways. Summer and fall frequently emerged as the dominant seasons across the study area, as seen in 2009 with fall (55% in N-1 and 61% in N-4) and 2017 with summer (77% in N-1 and 87% in S-4). Spring often contributed substantially, particularly during years of volcanic quiescence, such as 2016 (100% in C-2, 98% in S-1, and 89% in C-3). Winter contributions, while generally lower, remained significant in specific years and subregions, such as 2012 (74% in N-1, Jan-Feb 59%, Dec 15%) and 2010 (80% in C-4, Jan-Feb 19%, Dec 61%).

The regional breakdown reveals some distinct longitudinal fingerprints of aerosol transport and persistence across the European sector. Northern regions (N-1 to N-4) demonstrate a high sensitivity to high-latitude volcanic and boreal smoke signals, often showing a marked eastward intensification in seasonal impact; for instance, in 2008, fall contributions increased from 54% in N-1 to 89% in N-4. The Central regions (C-1 to C-4) act as a transition zone with extreme inter-annual variability, as seen in C-1 where the dominant season shifted from summer in 2014 (91%) to winter in 2022 (Jan-Feb: 84%). Southern regions (S-1 to S-4) display the most localized seasonal extremes and unique sensitivity to tropical or mid-

https://doi.org/10.5194/egusphere-2026-2307
Preprint. Discussion started: 8 May 2026

latitude injections, evidenced in 2013 when winter (Jan-Feb) accounted for 100% of the annual signal in S-2, and in 2011 when summer reached 95% in S-4.

This spatial and temporal heterogeneity underscores the complexity of stratospheric aerosol evolution as plumes dilute and evolve during their transit across different latitudinal and longitudinal bands. It is important to note, however, that these regional variations are likely to be influenced by the intersection of plume transport and satellite orbital geometry. The detection of a "peak" signal in a specific longitudinal subregion often depends on whether the satellite overpass coincides spatially and temporally with the maximum concentration of the aerosol layer, potentially leading to localized enhancements in the recorded sAOD.

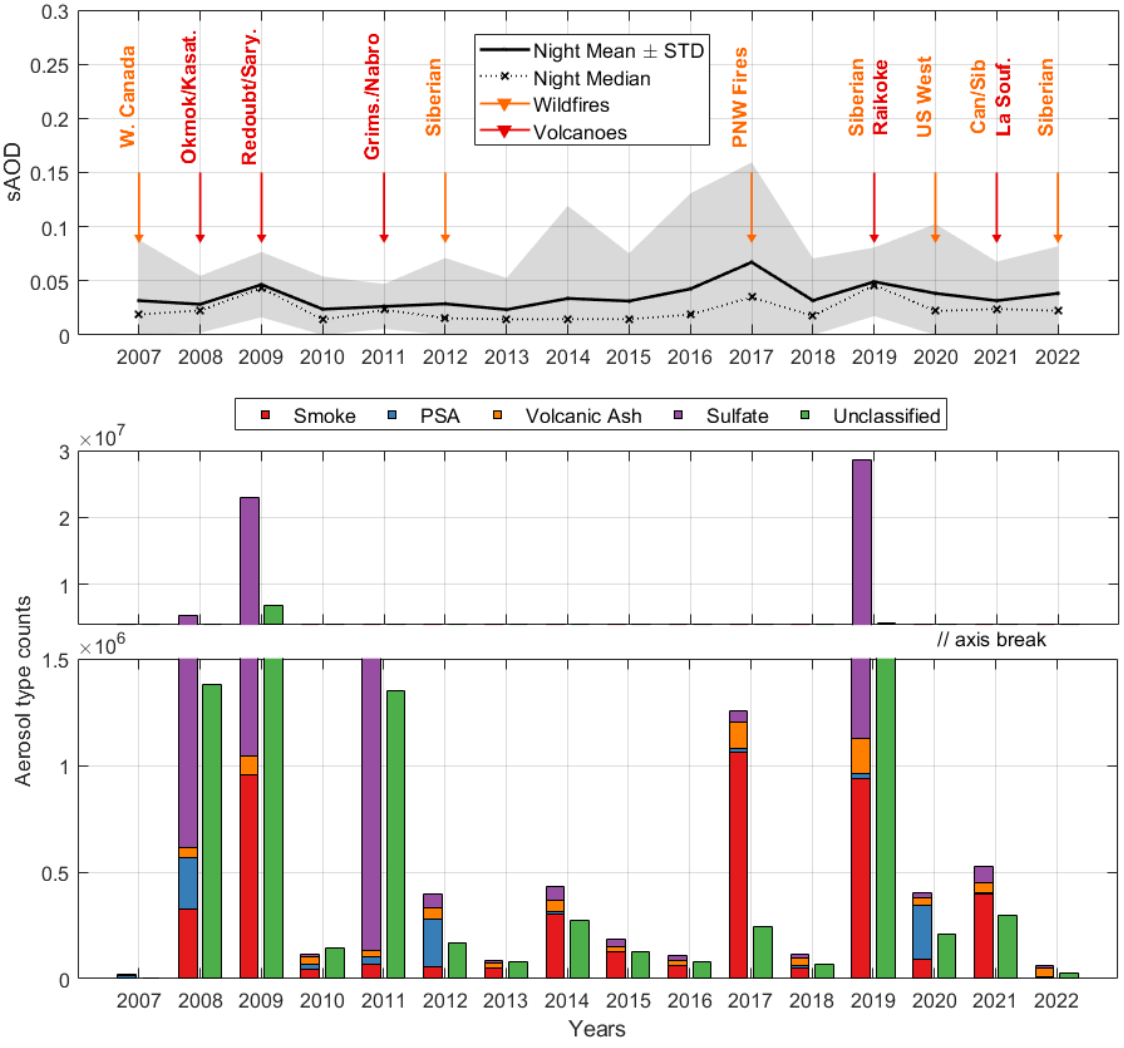

Figure 9: (Top) Time series of annual mean (solid lines) and median (dotted lines) sAOD nighttime observations; shaded area denotes the std. Vertical arrows highlight major stratospheric events: wildfire events (orange) and volcanic eruptions (red), corresponding to events listed in Table 1 and 2. (Bottom) Distribution of CALIPSO stratospheric aerosol subtype counts.

https://doi.org/10.5194/egusphere-2026-2307
Preprint. Discussion started: 8 May 2026

3.5 Seasonal Contributions to Total sAOD and type Attribution

By combining sAOD measurements with the seasonal distribution of aerosol subtypes (smoke, PSA, volcanic ash, sulfate, and unclassified) across all 12 subregions, we provide a unified characterization of stratospheric aerosols over a broad European domain. Figure 9 illustrates the annual variability of mean and median sAOD for nighttime observations over Europe from 2007 to 2022, together with the major wildfire and volcanic events.

The data captures the distinct influence of major volcanic and wildfire events over the 16-year period. The record begins in 2007, a year marked by the Western Canada fires, with a nighttime mean of 0.032 ± 0.006 (median 0.019). Following the high-latitude eruptions of Okmok and Kasatochi in 2008, the subsequent Sarychev Peak eruption in 2009 resulted in a notable increase in the nighttime mean to 0.047 ± 0.001 (median 0.043). During 2010 and 2011, which saw the eruptions of Grímsvötn, and Nabro, nighttime values remained relatively stable, potentially because these events primarily impacted the troposphere rather than the stratosphere (Mona et al., 2012; Papayannis et al., 2012; Zerefos et al., 2017; Tesche et al., 2012). A slight increase in 2012 is observable, likely due to Siberian fires, the nighttime mean was recorded at 0.029 ± 0.005 (median 0.016). Following a period of relative quiescence, a major peak is observed in 2017, directly attributed to the extreme Canadian wildfire (PNW) event; here, the nighttime mean reached 0.067 ± 0.009 (median 0.035). In 2019, the Raikoke eruption and Siberian wildfires led to a nighttime mean of 0.049 ± 0.001 (median 0.046). The record for 2020 and 2021 reflects a continued aerosol presence from the US West Coast and Siberian wildfires. Finally, in 2022, a second major peak driven by extensive Siberian wildfires resulted in a nighttime mean of 0.039 ± 0.006 (median 0.022).

In parallel with the annual sAOD variability described above, the distribution of seasonal contributions offers further insight into how specific volcanic eruptions and wildfire events shaped the aerosol burden over Europe, summarized in Fig. 10.

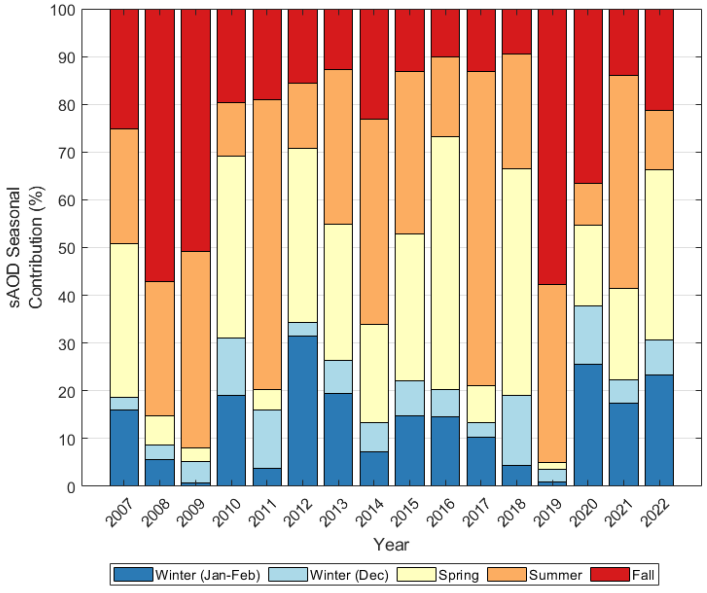

Figure 10: Seasonal percentage contribution to the sAOD for nighttime observations over Europe (2007-2022).

https://doi.org/10.5194/egusphere-2026-2307
Preprint. Discussion started: 8 May 2026

Years dominated by major wildfire activity show the strongest nighttime summer contributions, including 2017 (66%) during the PNW wildfire episode and 2021 (45%) following widespread US West Coast and Siberian fires, whereas the elevated contribution in 2011 (61%) is linked to aerosols from the Nabro eruption rather than wildfire activity. Spring contributions remain substantial during periods of enhanced aerosol transport, reaching 36% in 2012 and 47% in 2018. Winter shows pronounced interannual variability, again aligning with key events: contributions peak in 2012 (35%: Jan–Feb 32%, Dec 3%) and 2020 (38%: Jan–Feb 26%, Dec 12%), mirroring the influence of strong wintertime smoke transport from Siberia. Fall contributions become particularly elevated in 2009 (51%) and 2019 (58%), consistent with the lingering presence of volcanic aerosols from Sarychev Peak (2009) and Raikoke (2019), combined with widespread late-season Siberian burning.

Taken together, the seasonal contributions closely reflect the timing and intensity of the major volcanic eruptions and wildfire events documented in the interannual sAOD variability. Summers amplify the influence of large-scale wildfire smoke and volcanic plumes, Springs capture efficient secondary aerosol formation and long-range transport, and Winters display episodic yet event-linked enhancements. These seasonal patterns provide a complementary perspective to the annual means, reinforcing the central role of episodic natural events in shaping the temporal structure of sAOD over Europe throughout 2007–2022. Moreover, they are particularly distinct at night, as the behavior highlights features associated with the reduced influence of photochemistry.

To better understand the seasonal structure underlying the sAOD variability described above, we examine the seasonal contributions of the four major stratospheric aerosol subtypes: smoke, PSA, volcanic ash, and sulfate (Fig. 11). These subtype-specific patterns clarify which aerosol sources dominate in different seasons, observed in the sAOD record. Although some aerosol types follow physically meaningful seasonal cycles (e.g., PSA in winter, sulfate in summer), others, such as volcanic ash, reflect the timing of major eruptive events rather than recurring seasonal behavior.

3.5.1 Smoke aerosols

Smoke aerosols display the clearest connection to known wildfire events, characterized by a strong summer dominance in major fire years. In years heavily impacted by boreal or North American wildfires—such as 2013 (92%), 2014 (95%), 2015 (81%), 2017 (76%), and 2021 (95%)—summer contributions are the primary driver of the annual count. Spring becomes the leading season in years with early-season or significant Siberian fire activity, most notably in 2012 (72%), 2016 (97%), and 2022 (60%). Fall contributions strengthen in years with prolonged transport or late-season activity, particularly in 2008 (53%) and 2020 (83%). Winter contributions generally remain negligible but reached a notable 29% in 2022.

https://doi.org/10.5194/egusphere-2026-2307
Preprint. Discussion started: 8 May 2026

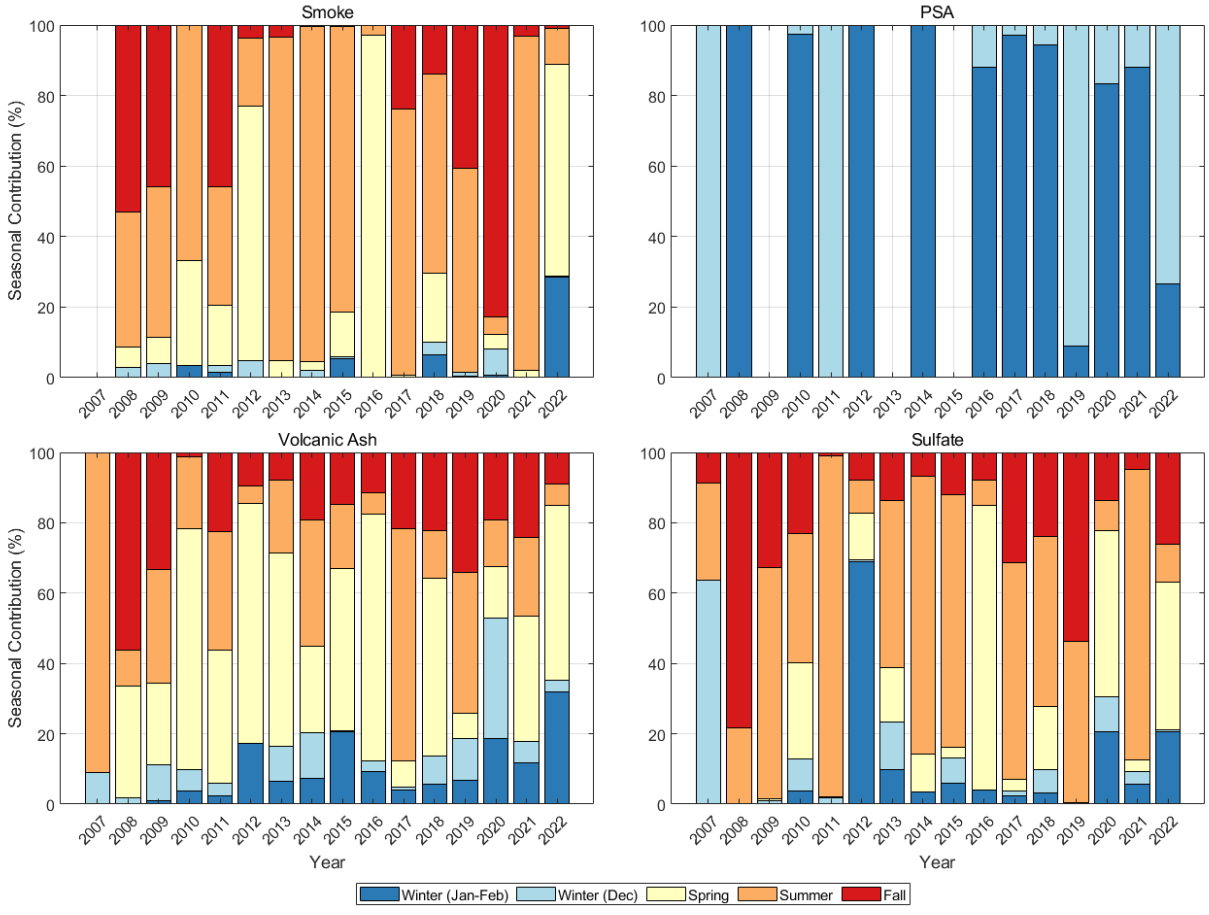

Figure 11: Seasonal percentage contribution of the four major stratospheric aerosol subtypes—smoke, PSA, volcanic ash, and sulfate—to the total detections over Europe for the period 2007–2022, for nighttime observations.

3.5.2 PSA aerosols

PSA aerosols exhibit the strongest seasonal confinement of all types, appearing exclusively during the winter months, as expected. Their presence reflects the cold stratospheric temperatures and polar vortex conditions typical of the mid-winter period. PSA is entirely winter-bound, with variability arising only from the relative dominance of the early (Jan–Feb) or late (December) winter periods. Jan–Feb-dominated years include 2010 (97%), 2012 (100%), 2014 (100%), and 2021 (88%). Conversely, December-dominated years include 2007 (100%), 2011 (100%), 2019 (91%), and 2022 (73%). No contributions are observed in spring, summer, or fall across the 16-year record. As PSA occurs independently of volcanic or wildfire activity, it provides a stable wintertime baseline that contributes to occasional winter enhancements in the overall sAOD record.

https://doi.org/10.5194/egusphere-2026-2307
Preprint. Discussion started: 8 May 2026

3.5.3 Volcanic Ash Aerosols

Volcanic ash contributions correspond directly to the timing of major eruptions. Peaks coincide with key events identified in the annual record: 2008–2009 (Okmok, Kasatochi, Sarychev Peak), 2011 (Grímsvötn), 2011 (Nabro), and 2019 (Raikoke). During these periods, seasonal dominance shifts according to the eruption date. Summer was the primary season in 2007 (91%), 2017 (66%), and 2019 (40%). Strong spring contributions are frequently observed, particularly in 2010 (68%), 2012 (68%), 2016 (70%), and 2022 (50%). Fall plays a secondary role but becomes significant during years with long-lived plumes, such as 2008 (56%) and 2019 (34%). Winter contributions increase when volcanic aerosol persists into the cold season, as seen in 2020 (53% combined).

3.5.4 Sulfate Aerosols

Sulfate aerosols demonstrate high seasonal variability, often driven by the photochemical production of sulfuric acid following volcanic sulfur dioxide injections. Summer dominance is evident in years such as 2009 (66%), 2011 (97%), 2014 (79%), 2015 (72%), and 2021 (82%). However, sulfate also shows a balanced seasonal structure with significant spring contributions, particularly in 2016 (81%), 2020 (47%), and 2022 (42%). Fall contributions were prominent in 2008 (78%) and 2019 (54%), reflecting the late-year persistence of sulfate layers. Winter becomes an important factor in specific years, such as 2012 (69%) and 2020 (31%), likely due to the trapping of sulfate aerosols within the polar vortex or late-season volcanic persistence.

3.6 sAOD Trend

Understanding the long-term evolution of stratospheric aerosols is critical for quantifying their role in the Earth's radiative budget. While the 16-year record provided by CALIOP represents an unprecedented dataset for vertical profiling, detecting a definitive climatic trend remains a challenge due to the high frequency of episodic injections. Figure 12 presents the time series of the mean annual nighttime sAOD (2007–2022) for the study region along with the weighted least squares (WLS) line. Because of the annual sAOD estimates exhibit large variability in sampling density and retrieval uncertainty, we applied a WLS regression using weights proportional to N/std^2. The weight choice enhances the contribution of well sampled and low variability years. sAOD exhibits a mean value of 0.036. The data yield a weak positive slope, +0.0008 sAOD/year, but not statistically significant (p=0.088)

https://doi.org/10.5194/egusphere-2026-2307
Preprint. Discussion started: 8 May 2026

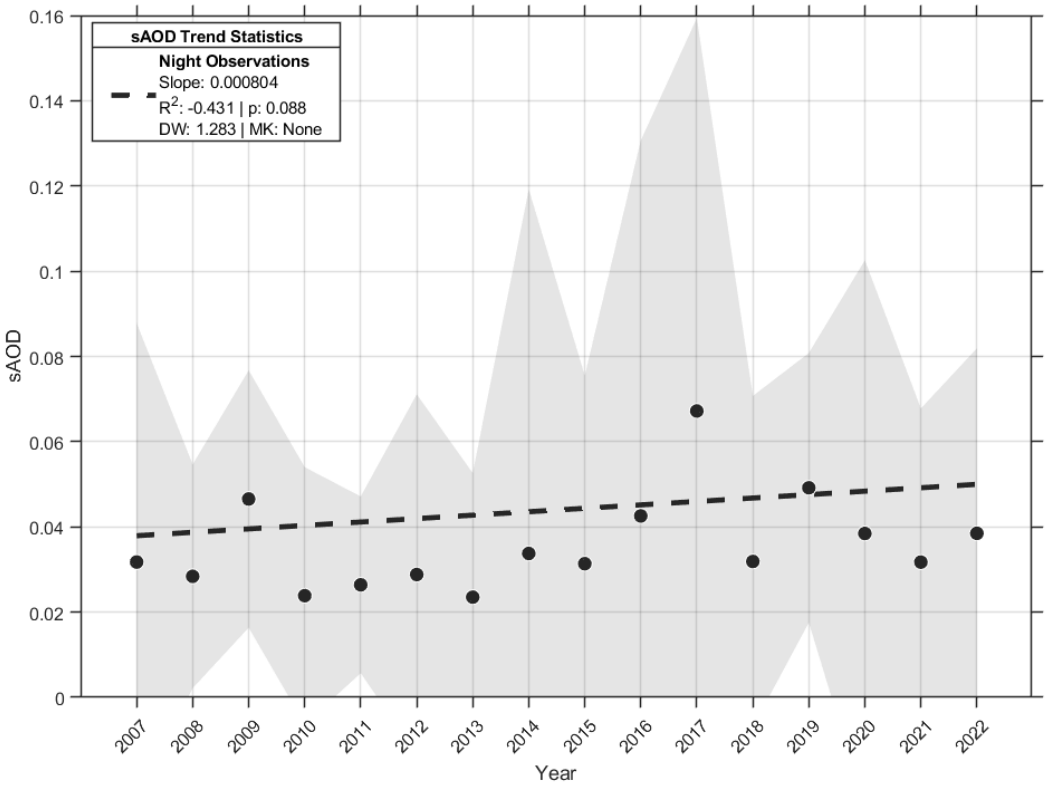

Figure 12. Time series of the nighttime mean annual sAOD (2007–2022) across the twelve European subregions combined. The shaded areas denote the standard deviation. The dashed line represents the WLS, (w = N/std^2) fit and the inset panel contains relative details as well as information on autocorrelation (DW) and non-parametric trend (MK) tests.

The lack of a significant trend is further validated by a Mann–Kendall (Kendall, 1975; Mann, 1945) analysis, which yielded an S-statistic of 35 (p = 0.088) and a consistent Theil–Sen slope (Sen, 1968) of 0.001. This marginal tendency remains stable even after accounting for the influence of extreme aerosol injections in 2017 and 2022. Furthermore, the Durbin-Watson (DW) statistic for the nighttime data (1.283) indicates a more persistent, autocorrelated signal compared to more transient daytime observations. This lower DW value suggests a degree of temporal dependence in the stratospheric background that further complicates trend detection in the nighttime record.

https://doi.org/10.5194/egusphere-2026-2307
Preprint. Discussion started: 8 May 2026

The structural shift in the sAOD is further elucidated by the Cumulative Sum (cusum) plot (Fig. 13). The cusum is calculated by taking the difference between each year's annual mean and the total 16-year long-term average (0.036) and summing these differences chronologically starting from 2007. By accumulating these deviations from the mean over time, the cusum reveals sustained shifts in the aerosol regime.

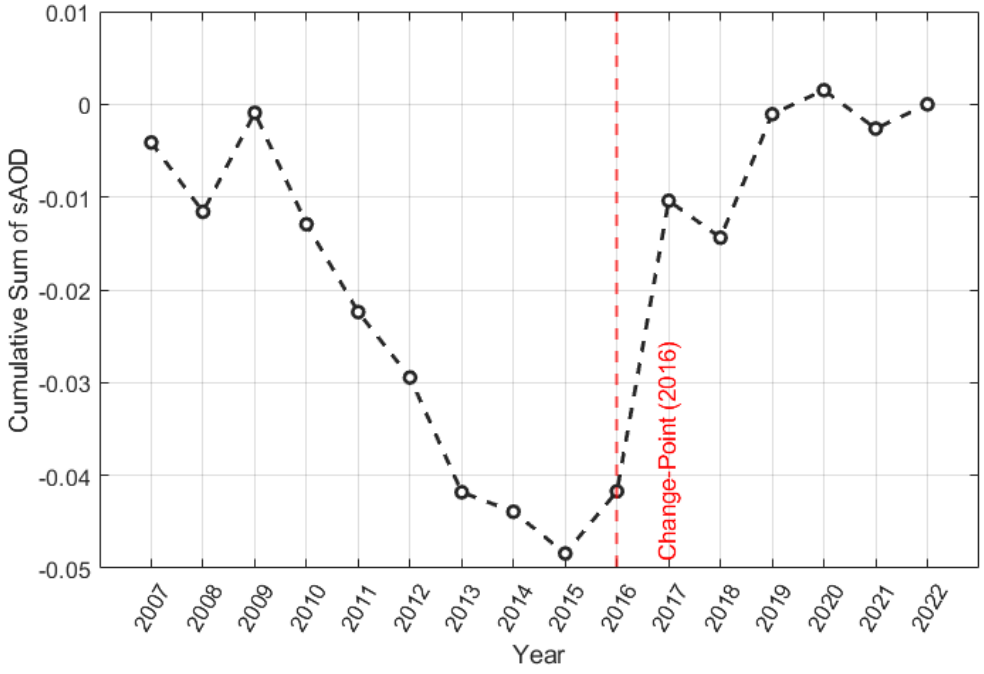

Figure 13: Cumulative Sum (cusum) of annual nighttime sAOD deviations from the long-term mean (2007–2022). The curve represents the chronological accumulation of the difference between each year's annual mean and the 16-year average (0.036). A sustained positive slope in the cusum curve indicates a period where sAOD values consistently exceeded this long-term average, marking a transition toward a higher stratospheric aerosol loading regime after 2016.

The resulting curve suggests a prominent change-point around 2016; while the period from 2007 to 2015 is characterized by a steady decrease in the cumulative sum, the subsequent sharp upward inflection denotes a transition to a higher-loading regime. This 2016 transition aligns with an era of increased frequency in moderate-scale volcanic eruptions and extreme pyroconvective wildfire events, confirming that the nighttime stratospheric background has shifted toward a sustained higher-loading state rather than being driven by isolated, transient events.

4 Conclusions

This study uses a complete 16-year nighttime CALIPSO data record (2007-2022) and the updated stratospheric typing algorithm following (Tackett et al., 2023) to depict the seasonal and interannual characteristics of stratospheric aerosol over Europe. The CALIPSO record provides a detailed view of how the European stratosphere responds to a sequence of volcanic injections, pyroCb driven wildfire intrusions, and large-scale transport processes. When examined across the twelve

https://doi.org/10.5194/egusphere-2026-2307
Preprint. Discussion started: 8 May 2026

subregions spanning southern to northern Europe, we found that the European stratosphere has transitioned into a highly dynamic, event-driven regime, where the frequency and vertical extent of aerosol intrusions have increased significantly over the decade. A consistent spatial structure emerged, northern latitudes experienced the most frequent and most persistent aerosol layers, central Europe showed intermediate behavior, and the southern subregions are characterized by weaker, more diluted layers. This gradient reflects not only the satellite's sampling geometry but also the the large-scale transport by the Brewer–Dobson circulation, transporting aerosols from the tropics and mid-latitudes toward the poles, leading to a long-term accumulation and higher residence times in the lower stratosphere of the high latitudes (Kloss et al., 2021).

Interannual variability is dominated by a small number of powerful events. The early years (2008–2009) were shaped by the eruptions of Okmok, Kasatochi, and Sarychev Peak which led to clear and coherent enhancements across almost all northern and central subregions. The period 2010–2012 reflects influences from Grímsvötn, Nabro, and repeated Siberian fire seasons, producing elevated sulfate and mixed aerosol layers that lingered for extended periods. A second major phase begins in 2017, marked by the exceptionally intense PNW (Ansmann et al., 2018; Baars et al., 2018; Hu et al., 2019; Haarig et al., 2018) wildfires, followed by large injection from Raikoke in 2019 (Trickl et al., 2024; Ansmann et al., 2021a; Voudouri et al., 2023) and multiple years of Siberian and North American wildfires from 2019 to 2022, also observed by ground-based lidar stations across Europe, which documented the arrival and persistence of the plumes throughout these years (Ansmann et al., 2021a; Baars et al., 2021).

The analysis of the vertical distribution of the stratospheric aerosols revealed a progressive increase in the altitude and vertical extend of these aerosols over time, frequently reaching heights of 17–19 km in the latter years of the study. This trend is directly linked to the increasing potency of pyroCb events (Peterson et al., 2025, 2018b; Khaykin et al., 2020), which now rival moderate volcanic eruptions in their ability to perturb the mid-latitude stratosphere. The seasonal cycle further reflects these physical drivers: summer and spring dominate due to wildfire smoke and efficient transport; PSA appears during winter, and the imprint of long-lived volcanic or smoke plumes becomes most apparent in autumn. The subtype distribution reinforces these patterns, with sulfate dominating and smoke peaking sharply during major fire years. The record captured the distinct influence of these events through annual mean nighttime sAOD values, which varied from 0.032 in the early years (2007) to a major peak of 0.067 in 2017 following the PNW event, before settling at 0.039 in 2022, despite extensive Siberian fire activity.

While the European stratosphere appears increasingly event-driven, the 16-year record from 2007 to 2022 offers a relatively narrow window for definitive climatic trend analysis (Fromm et al., 2022). Despite the weak and statistically insignificant sAOD increase, the cusum analysis revealed a prominent change-point after 2016. This finding aligns with the "new era" of elevated aerosol phase which began in 2017 with the exceptionally violent PNW wildfires and has been widely documented (Trickl et al., 2024; Tackett et al., 2023; Kar et al., 2019; Fromm et al., 2019, 2022). This shift indicates an important change in the aerosol "baseline" for Europe, with significant implications for long-term climate modeling and regional atmospheric stability. Nonetheless, this suggestive trend, although not significant, requires an expansive record of aerosol profiles in the stratosphere forward in time. Since CALIPSO operations ceased in August 2023, the path forward is EarthCARE, a joint

https://doi.org/10.5194/egusphere-2026-2307
Preprint. Discussion started: 8 May 2026

ESA-JAXA mission, that was launched on 28 May 2024 (Donovan et al., 2024) and equipped with a high spectral resolution lidar called ATLID (Atmospheric Lidar) gives the impetus for further studies. Whilst its design lifetime was around 3 years, ESA-JAXA's current assessment indicates potential for ≥10 years of operations (targeting ~2034 and beyond), providing the temporal leverage that a 16-year CALIPSO climatology alone cannot offer for separating regime shifts, decadal variability, and emerging trends.

The methodology developed in this study provides a robust framework for the monitoring of stratospheric aerosols through the years, offering a scalable approach to quantify the impact of extreme or moderate injection events on atmospheric composition, by providing this multi-year dataset of observations of the European stratospheric aerosol load and types. Furthermore, our methodology is designed to be applied to other regions to provide a consistent global perspective. Expanding this analysis to other areas of interest, and specifically to the Arctic would be especially valuable, given the region's sensitivity, long aerosol residence times, and increasing exposure to high-latitude wildfires and volcanic sources. Such an expansion would not only help assess hemispheric transport and aerosol evolution but also contribute to a broader understanding of how a rapidly changing climate is reshaping the composition and behaviour of the global stratosphere (Zhong et al., 2026).

Data availability

The CALIPSO Level 2 Aerosol Profile (APro) and Vertical Feature Mask (VFM) data used in this study were obtained from the NASA Langley Research Center Atmospheric Science Data Center (ASDC). These data are publicly available and can be accessed through the ASDC portal at: https://asdc.larc.nasa.gov/project/CALIPSO (last access: 16 April 2026).

Supplement link

The link to the supplement will be included by Copernicus, if applicable.

Author contributions

Conceptualization, C.-A.P. and N.P.; methodology, C.-A.P. and N.P.; software, C.-A.P.; formal analysis, C.-A.P.; investigation, C.-A.P. and N.P.; data curation, C.-A.P.; writing—original draft preparation, C.-A.P. and N.P.; writing—review and editing, C.-A.P., N.P., M.M., P.G-C, B.D.R., A. A., G.D., L.M; visualization, C.-A.P. and N.P.; funding acquisition, L.M. All authors have read and agreed to the published version of the manuscript.

Competing interests

The authors declare that they have no conflict of interest.

https://doi.org/10.5194/egusphere-2026-2307
Preprint. Discussion started: 8 May 2026

Disclaimer

Copernicus Publications remains neutral with regard to jurisdictional claims made in the text, published maps, institutional affiliations, or any other geographical representation in this paper. While Copernicus Publications makes every effort to include appropriate place names, the final responsibility lies with the authors. Views expressed in the text are those of the authors and do not necessarily reflect the views of the publisher.

Acknowledgements

The authors would like to acknowledge ACTRIS-IT and ITINERIS (IR0000032; CUP: B53C22002150006) for the research infrastructure and support provided. This study was supported by the PER-ACTRIS-IT project (No. CIR01_00015, No. 2595; CUP: B58I20000220001) funded by the EU – Next Generation EU PNRR. We also acknowledge the NASA ASDC for providing the CALIPSO data.

Financial support

This research has been supported by MUR (Italian Ministry of University and Research) through the following projects: ITINERIS, the Italian Integrated Environmental Research Infrastructure System (grant no. IR0000032, D.D. no. 130/2022 – CUP B53C22002150006), which is funded by the European Union under Next Generation EU – PNRR Mission 4, Component 2, Investment 3.1: Fund for the realization of an integrated system of research and innovation infrastructures) and PER-ACTRIS-IT CIR01_00015, CUP F88I2000019000, which is funded by the European Regional Development Fund.

Review statement

The review statement will be added by Copernicus Publications listing the handling editor as well as all contributing referees according to their status anonymous or identified.

References

Allen, D. R., Fromm, M. D., Kablick III, G. P., and Nedoluha, G. E.: Smoke with Induced Rotation and Lofting (SWIRL) in the Stratosphere, J. Atmos. Sci., 77, 4297–4316, https://doi.org/https://doi.org/10.1175/JAS-D-20-0131.1, 2020.

Ansmann, A., Seifert, P., Tesche, M., and Wandinger, U.: Profiling of fine and coarse particle mass: Case studies of Saharan dust and Eyjafjallajökull/Grimsvötn volcanic plumes, Atmos. Chem. Phys., 12, 9399–9415, https://doi.org/10.5194/acp-12-9399-2012, 2012.

https://doi.org/10.5194/egusphere-2026-2307
Preprint. Discussion started: 8 May 2026

Ansmann, A., Baars, H., Chudnovsky, A., Mattis, I., Veselovskii, I., Haarig, M., Seifert, P., Engelmann, R., and Wandinger, U.: Extreme levels of Canadian wildfire smoke in the stratosphere over central Europe on 21-22 August 2017, Atmos. Chem. Phys., 18, 11831–11845, https://doi.org/10.5194/acp-18-11831-2018, 2018.

Ansmann, A., Ohneiser, K., Chudnovsky, A., Baars, H., and Engelmann, R.: CALIPSO Aerosol-Typing Scheme Misclassified Stratospheric Fire Smoke: Case Study From the 2019 Siberian Wildfire Season, Front. Environ. Sci., 9, 1–14, https://doi.org/10.3389/fenvs.2021.769852, 2021a.

Ansmann, A., Ohneiser, K., Mamouri, R. E., Knopf, D. A., Veselovskii, I., Baars, H., Engelmann, R., Foth, A., Jimenez, C., Seifert, P., and Barja, B.: Tropospheric and stratospheric wildfire smoke profiling with lidar: Mass, surface area, CCN, and INP retrieval, Atmos. Chem. Phys., 21, 9779–9807, https://doi.org/10.5194/acp-21-9779-2021, 2021b.

Ansmann, A., Ohneiser, K., Chudnovsky, A., Knopf, D. A., Eloranta, E. W., Villanueva, D., Seifert, P., Radenz, M., Barja, B., Zamorano, F., Jimenez, C., Engelmann, R., Baars, H., Griesche, H., Hofer, J., Althausen, D., and Wandinger, U.: Ozone depletion in the Arctic and Antarctic stratosphere induced by wildfire smoke, Atmos. Chem. Phys., 22, 11701–11726, https://doi.org/10.5194/acp-22-11701-2022, 2022.

Aubry, T. J., Staunton-Sykes, J., Marshall, L. R., Haywood, J., Abraham, N. L., and Schmidt, A.: Climate change modulates the stratospheric volcanic sulfate aerosol lifecycle and radiative forcing from tropical eruptions, Nat. Commun., 12, https://doi.org/10.1038/s41467-021-24943-7, 2021.

Baars, H., Ansmann, A., Ohneiser, K., Haarig, M., Engelmann, R., Althausen, D., Hanssen, I., Gausa, M., Pietruczuk, A., Szkop, A., Stachlewska, S., Wang, D., Reichardt, J., Skupin, A., Mattis, I., Trickl, T., Vogelmann, H., Navas-guzmán, F., Haefele, A., Acheson, K., and Ruth, A. A.: The unprecedented 2017 – 2018 stratospheric smoke event : Decay phase and aerosol properties observed with EARLINET, 2018.

Baars, H., Ansmann, A., Ohneiser, K., Haarig, M., Engelmann, R., Althausen, D., Hanssen, I., Gausa, M., Pietruczuk, A., Szkop, A., Stachlewska, I. S., Wang, D., Reichardt, J., Skupin, A., Mattis, I., Trickl, T., Vogelmann, H., and Navas-guzmán, F.: The unprecedented 2017 – 2018 stratospheric smoke event : decay phase and aerosol properties observed with the EARLINET, 15183–15198, 2019.

Bègue, N., Vignelles, D., Berthet, G., Portafaix, T., Payen, G., Jégou, F., Benchérif, H., Jumelet, J., Vernier, J., Lurton, T., Renard, J., Clarisse, L., Duverger, V., Posny, F., Metzger, J., and Godin-beekmann, S.: Long-range transport of stratospheric aerosols in the Southern Hemisphere following the 2015 Calbuco eruption, 15019–15036, 2017.

Boucher, O.: Atmospheric Aerosols, in: Atmospheric Aerosols: Properties and Climate Impacts, Springer Netherlands, Dordrecht, 9–24, https://doi.org/10.1007/978-94-017-9649-1_2, 2015.

Bruckert, J., Hirsch, L., Horváth, Á., Kahn, R. A., Kölling, T., and Muser, L. O.: Dispersion and Aging of Volcanic Aerosols

https://doi.org/10.5194/egusphere-2026-2307
Preprint. Discussion started: 8 May 2026

After the La Soufrière Eruption in April 2021 Journal of Geophysical Research : Atmospheres, https://doi.org/10.1029/2022JD037694, 2023.

Bull, K. F. and Buurman, H.: An overview of the 2009 eruption of Redoubt Volcano , Alaska, J. Volcanol. Geotherm. Res., 259, 2–15, https://doi.org/10.1016/j.jvolgeores.2012.06.024, 2013.

Cheremisin, A. A., Marichev, V. N., Bochkovskii, D. A., Novikov, P. V, and Romanchenko, I. I.: Stratospheric Aerosol of Siberian Forest Fires According to Lidar Observations in Tomsk in August 2019, 35, 57–64, https://doi.org/10.1134/S1024856022010043, 2022.

Christian, K., Wang, J., Ge, C., Peterson, D., Hyer, E., Yorks, J., and McGill, M.: Radiative Forcing and Stratospheric Warming of Pyrocumulonimbus Smoke Aerosols: First Modeling Results With Multisensor (EPIC, CALIPSO, and CATS) Views from Space, Geophys. Res. Lett., 46, 10061–10071, https://doi.org/10.1029/2019GL082360, 2019.

Clarisse, L., Theys, N., Hurtmans, D., and Clerbaux, C.: The 2011 Nabro eruption , a SO 2 plume height analysis using IASI measurements, 2001, 3095–3111, https://doi.org/10.5194/acp-14-3095-2014, 2014.

Das, S., Colarco, P. R., Oman, L. D., Taha, G., and Torres, O.: The long-term transport and radiative impacts of the 2017 British Columbia pyrocumulonimbus smoke aerosols in the stratosphere, Atmos. Chem. Phys., 21, 12069–12090, https://doi.org/10.5194/acp-21-12069-2021, 2021.

Domeisen, D. I. V. and Butler, A. H.: Stratospheric drivers of extreme events at the Earth's surface, Commun. Earth Environ., 1, 1–8, https://doi.org/10.1038/s43247-020-00060-z, 2020.

Donovan, D. P., Zadelhoff, G. Van, and Wang, P.: The EarthCARE lidar cloud and aerosol profile processor (A-PRO):, 5301–5340, 2024.

Fromm, M.: The Untold Story of Pyrocumulonimbus, 1193–1210, https://doi.org/10.1175/2010BAMS3004.1, 2010.

Fromm, M., Peterson, D., and Di Girolamo, L.: The Primary Convective Pathway for Observed Wildfire Emissions in the Upper Troposphere and Lower Stratosphere: A Targeted Reinterpretation, J. Geophys. Res. Atmos., 124, 13254–13272, https://doi.org/https://doi.org/10.1029/2019JD031006, 2019.

Fromm, M., Servranckx, R., Peterson, D. A., and Stocks, B. J.: Understanding the critical elements of the pyrocumulonimbus storm sparked by high-intensity wildland fire, 1–7, https://doi.org/10.1038/s43247-022-00566-8, 2022.

Fu, Q., White, R. H., Wang, M., Alexander, B., Solomon, S., Gettelman, A., Battisti, D. S., and Lin, P.: The Brewer - Dobson Circulation During the Last Glacial Maximum Geophysical Research Letters, 1–10, https://doi.org/10.1029/2019GL086271, 2020.

Grebennikov, V. S., Zubachev, D. S., Korshunov, V. A., Sakhibgareev, D. G., and Chernikh, I. A.: Observations of Stratospheric Aerosol at Rosgidromet Lidar Stations after the Eruption of the Raikoke Volcano in June 2019, 33, 519–523, https://doi.org/10.1134/S1024856020050097, 2020.

Haarig, M., Ansmann, A., Baars, H., Jimenez, C., Veselovskii, I., Engelmann, R., and Althausen, D.: Depolarization and lidar ratios at 355, 532, and 1064 nm and microphysical properties of aged tropospheric and stratospheric Canadian wildfire smoke, Atmos. Chem. Phys., 18, 11847–11861, https://doi.org/10.5194/acp-18-11847-2018, 2018.

https://doi.org/10.5194/egusphere-2026-2307
Preprint. Discussion started: 8 May 2026

Halofsky, J. E., Peterson, D. L., and Harvey, B. J.: Changing wildfire, changing forests: the effects of climate change on fire regimes and vegetation in the Pacific Northwest, USA, Fire Ecol., 16, https://doi.org/10.1186/s42408-019-0062-8, 2020.

Hirsch, E. and Koren, I.: Record-breaking aerosol levels explained by smoke injection into the stratosphere, Science (80-.)., 371, 1269–1274, https://doi.org/10.1126/science.abe1415, 2021.

Hoffmann, A., Ritter, C., Stock, M., Maturilli, M., Eckhardt, S., Herber, A., and Neuber, R.: Lidar measurements of the Kasatochi aerosol plume in August and September 2008 in Ny - Ålesund , Spitsbergen, 115, 1–12, https://doi.org/10.1029/2009JD013039, 2010.

Hu, Q., Goloub, P., Veselovskii, I., Bravo-Aranda, J. A., Elisabeta Popovici, I., Podvin, T., Haeffelin, M., Lopatin, A., Dubovik, O., Pietras, C., Huang, X., Torres, B., and Chen, C.: Long-range-transported Canadian smoke plumes in the lower stratosphere over northern France, Atmos. Chem. Phys., 19, 1173–1193, https://doi.org/10.5194/acp-19-1173-2019, 2019.

Kablick, G. P., Allen, D. R., Fromm, M. D., and Nedoluha, G. E.: Australian PyroCb Smoke Generates Synoptic-Scale Stratospheric Anticyclones, Geophys. Res. Lett., 47, https://doi.org/10.1029/2020GL088101, 2020.

Kar, J., Lee, K., Vaughan, M. A., Tackett, J. L., Trepte, C. R., Winker, D. M., Lucker, P. L., and Getzewich, B. J.: CALIPSO level 3 stratospheric aerosol profile product : version 1 . 00 algorithm description and initial assessment, 6173–6191, 2019.

Kendall, M. G.: Rank Correlation Methods, 4th Edition., Charles Griffin, London, UK, 1975.

Khaykin, S., Legras, B., Bucci, S., Sellitto, P., Isaksen, L., Tencé, F., Bekki, S., Bourassa, A., Rieger, L., Zawada, D., Jumelet, J., and Godin-Beekmann, S.: The 2019/20 Australian wildfires generated a persistent smoke-charged vortex rising up to 35 km altitude, Commun. Earth Environ., 1, 1–12, https://doi.org/10.1038/s43247-020-00022-5, 2020.

Khaykin, S. M., de Laat, A. T. J., Godin-Beekmann, S., Hauchecorne, A., and Ratynski, M.: Unexpected self-lofting and dynamical confinement of volcanic plumes: the Raikoke 2019 case, Sci. Rep., 12, 1–12, https://doi.org/10.1038/s41598-022-27021-0, 2022.

Kim, M. H., Omar, A. H., Tackett, J. L., Vaughan, M. A., Winker, D. M., Trepte, C. R., Hu, Y., Liu, Z., Poole, L. R., Pitts, M. C., Kar, J., and Magill, B. E.: The CALIPSO version 4 automated aerosol classification and lidar ratio selection algorithm, Atmos. Meas. Tech., 11, 6107–6135, https://doi.org/10.5194/amt-11-6107-2018, 2018.

Kloss, C., Berthet, G., Sellitto, P., Ploeger, F., Taha, G., Tidiga, M., Eremenko, M., Bossolasco, A., Jégou, F., Renard, J., and Legras, B.: Stratospheric aerosol layer perturbation caused by the 2019 Raikoke and Ulawun eruptions and climate impact, 1–33, 2020.

Kloss, C., Berthet, G., Sellitto, P., Ploeger, F., Taha, G., Tidiga, M., Eremenko, M., Bossolasco, A., Jégou, F., Renard, J., and Legras, B.: Stratospheric aerosol layer perturbation caused by the 2019 Raikoke and Ulawun eruptions and their radiative forcing, 535–560, 2021.

Kloss, C., Sellitto, P., Renard, J., Baron, A., Bègue, N., Legras, B., Briaud, E., Carboni, E., Duchamp, C., Duflot, V., Jacquet, P., Marquestaut, N., Metzger, J.-M., Payen, G., Ranaivombola, M., Roberts, T., Siddans, R., and Jegou, F.: Aerosol characterization of the stratospheric plume from the volcanic eruption at Hunga Tonga January 15 th 2022, Geophys. Res. Lett., 49, https://doi.org/10.1029/2022GL099394, 2022.

https://doi.org/10.5194/egusphere-2026-2307
Preprint. Discussion started: 8 May 2026

Kristiansen, N. I., Stohl, A., Prata, A. J., Richter, A., Eckhardt, S., Seibert, P., Hoffmann, A., Ritter, C., Bitar, L., Duck, T. J., and Stebel, K.: Remote sensing and inverse transport modeling of the Kasatochi eruption sulfur dioxide cloud, 115, 1–18, https://doi.org/10.1029/2009JD013286, 2010.

Ma, J., Chen, W., Yang, R., Ma, T., and Shen, X.: Downward propagation of the weak stratospheric polar vortex events : the role of the surface arctic oscillation and the quasi-biennial oscillation, 4117–4131, 2024.

Mamouri, R. E., Ansmann, A., Ohneiser, K., Knopf, D. A., Nisantzi, A., Bühl, J., Engelmann, R., Skupin, A., Seifert, P., Baars, H., Ene, D., Wandinger, U., and Hadjimitsis, D.: Wildfire smoke triggers cirrus formation: Lidar observations over the eastern Mediterranean, Atmos. Chem. Phys., 23, 14097–14114, https://doi.org/10.5194/acp-23-14097-2023, 2023.

Mann, H. B.: Nonparametric Tests Against Trend, Econometrica, 13, 245–259, https://doi.org/10.2307/1907187, 1945.

Mattis, I., Siefert, P., Müller, D., Tesche, M., Hiebsch, A., Kanitz, T., Schmidt, J., Finger, F., Wandinger, U., and Ansmann, A.: Volcanic aerosol layers observed with multiwavelength Raman lidar over central Europe in 2008-2009, J. Geophys. Res. Atmos., 115, 1–9, https://doi.org/10.1029/2009JD013472, 2010.

Min, Y., Ho, D., and Müller, D.: Variation of the vertical distribution of Nabro volcano aerosol layers in the stratosphere observed by LIDAR, Atmos. Environ., 154, 1–8, https://doi.org/10.1016/j.atmosenv.2017.01.033, 2017.

Mona, L., Amodeo, A., D'Amico, G., Giunta, A., Madonna, F., and Pappalardo, G.: Multi-wavelength Raman lidar observations of the Eyjafjallajökull volcanic cloud over Potenza, southern Italy, Atmos. Chem. Phys., 12, 2229–2244, https://doi.org/10.5194/acp-12-2229-2012, 2012.

Newhall, G. and Self, S.: The Volcanic Explosivity Index (VEI)' An Estimate of Explosive Magnitude for Historical Volcanism, 87, 1231–1238, 1982.

Ohneiser, K., Ansmann, A., Chudnovsky, A., Engelmann, R., Ritter, C., Veselovskii, I., Baars, H., Gebauer, H., Griesche, H., Radenz, M., Hofer, J., Althausen, D., Dahlke, S., and Maturilli, M.: The unexpected smoke layer in the High Arctic winter stratosphere during MOSAiC 2019-2020, Atmos. Chem. Phys., 21, 15783–15808, https://doi.org/10.5194/acp-21-15783-2021, 2021.

Papagiannopoulos, N., Mona, L., Alados-Arboledas, L., Amiridis, V., Baars, H., Binietoglou, I., Bortoli, D., D'Amico, G., Giunta, A., Luis Guerrero-Rascado, J., Schwarz, A., Pereira, S., Spinelli, N., Wandinger, U., Wang, X., and Pappalardo, G.: CALIPSO climatological products: Evaluation and suggestions from EARLINET, Atmos. Chem. Phys., 16, 2341–2357, https://doi.org/10.5194/acp-16-2341-2016, 2016.

Papanikolaou, C., Kokkalis, P., Soupiona, O., Solomos, S., Papayannis, A., Mylonaki, M., Anagnou, D., Foskinis, R., and Gidarakou, M.: Australian Bushfires (2019 – 2020): Aerosol Optical Properties and Radiative Forcing, 2022.

Papayannis, A., Mamouri, R. E., Amiridis, V., Giannakaki, E., Veselovskii, I., Kokkalis, P., Tsaknakis, G., Balis, D., Kristiansen, N. I., Stohl, A., Korenskiy, M., Allakhverdiev, K., Huseyinoglu, M. F., and Baykara, T.: Optical properties and vertical extension of aged ash layers over the Eastern Mediterranean as observed by Raman lidars during the Eyjafjallajökull eruption in May 2010, Atmos. Environ., 48, 56–65, https://doi.org/10.1016/j.atmosenv.2011.08.037, 2012.

Pappalardo, G., Amodeo, A., Apituley, A., Comeron, A., Freudenthaler, V., Linné, H., Ansmann, A., Bösenberg, J.,

https://doi.org/10.5194/egusphere-2026-2307
Preprint. Discussion started: 8 May 2026

D'Amico, G., Mattis, I., Mona, L., Wandinger, U., Amiridis, V., Alados-Arboledas, L., Nicolae, D., and Wiegner, M.: EARLINET: Towards an advanced sustainable European aerosol lidar network, Atmos. Meas. Tech., 7, 2389–2409, https://doi.org/10.5194/amt-7-2389-2014, 2014.

Peterson, D. A., Campbell, J. R., Hyer, E. J., Fromm, M. D., Iii, G. P. K., Cossuth, J. H., and Deland, M. T.: Wild fi re-driven thunderstorms cause a volcano-like stratospheric injection of smoke, npj Clim. Atmos. Sci., 1–8, https://doi.org/10.1038/s41612-018-0039-3, 2018a.

Peterson, D. A., Campbell, J. R., Hyer, E. J., Fromm, M. D., Kablick, G. P., Cossuth, J. H., and DeLand, M. T.: Wildfire-driven thunderstorms cause a volcano-like stratospheric injection of smoke, npj Clim. Atmos. Sci., 1, 1–8, https://doi.org/10.1038/s41612-018-0039-3, 2018b.

Peterson, D. A., Berman, M. T., Fromm, M. D., Servranckx, R., Julstrom, W. J., Hyer, E. J., Campbell, J. R., Mchardy, T. M., and Lambert, A.: Worldwide inventory reveals the frequency and variability of pyrocumulonimbus and stratospheric smoke plumes during 2013 – 2023, 2025.

Di Pierro, M., Jaeglé, L., Eloranta, E. W., and Sharma, S.: Spatial and seasonal distribution of Arctic aerosols observed by the CALIOP satellite instrument (2006-2012), Atmos. Chem. Phys., 13, 7075–7095, https://doi.org/10.5194/acp-13-7075-2013, 2013.

Popovicheva, O. B., Chichaeva, M. A., Evangeliou, N., Eckhardt, S., Diapouli, E., Kasimov, N. S., and Evangeliou, C. N.: Multi-year black carbon observations and modeling close to the largest gas flaring and wildfire regions in the Western Siberian Arctic, 7719–7739, 2025.

Prata, F., Woodhouse, M., Huppert, H. E., Prata, A., Thordarson, T., and Carn, S.: Atmospheric processes affecting the separation of volcanic ash and SO 2 in volcanic eruptions : inferences from the May 2011 Grímsvötn eruption, 10709–10732, 2017.

Proestakis, E., Gkikas, A., Georgiou, T., Kampouri, A., and Drakaki, E.: A near-global multiyear climate data record of the fine-mode and coarse-mode components of atmospheric pure dust, 3625–3667, 2024.

Sawamura, P., Vernier, J.P., Barnes, J.E., Berkoff, T.A., Welton, E.J., Alados-Arboledas, L., Navas-Guzmán, F., Pappalardo, G., Mona, L., Madonna, F., Lange, D., Sicard, M., Godin-Beekmann, S., Payen, G., Wang, Z., Hu, S., Tripathi,S.N., Cordoba-Jabonero, C., and Hoff, R.M.: Stratospheric AOD after the 2011 eruption of Nabro volcano measured by lidars over the Northern Hemisphere, Environ. Res. Lett., 7, 034013, https://doi.org/10.1088/1748-9326/7/3/034013, 2012.

Schallock, J., Brühl, C., Bingen, C., Höpfner, M., and Rieger, L.: Reconstructing volcanic radiative forcing since 1990 , using a comprehensive emission inventory and spatially resolved sulfur injections from satellite data in a chemistry-climate model, 1169–1207, 2023.

Schmale, J., Schneider, J., Jurkat, T., Voigt, C., Kalesse, H., Rautenhaus, M., Lichtenstern, M., Schlager, H., Ancellet, G., Arnold, F., Gerding, M., Mattis, I., Wendisch, M., and Borrmann, S.: Aerosol layers from the 2008 eruptions of Mount Okmok and Mount Kasatochi : In situ upper troposphere and lower stratosphere measurements of sulfate and organics over Europe, 115, 1–18, https://doi.org/10.1029/2009JD013628, 2010.

https://doi.org/10.5194/egusphere-2026-2307
Preprint. Discussion started: 8 May 2026

Sen, P. K.: Estimates of the Regression Coefficient Based on Kendall's Tau, J. Am. Stat. Assoc., 63, 1379–1389, https://doi.org/10.1080/01621459.1968.10480934, 1968.

Senf, F., Heinold, B., Kubin, A., Müller, J., Schrödner, R., and Tegen, I.: How the extreme 2019 – 2020 Australian wildfires affected global circulation and adjustments, 8939–8958, 2023.

Sharma, A. R., Acuna, D. C., and Abatzoglou, J. T.: Record-breaking fi re weather in North America in 2021 was initiated by the Paci fi c northwest heat dome, https://doi.org/10.1038/s43247-024-01346-2, 2024.

Tackett, J. L., Winker, D. M., Getzewich, B. J., Vaughan, M. A., Young, S. A., and Kar, J.: CALIPSO lidar level 3 aerosol profile product: Version 3 algorithm design, Atmos. Meas. Tech., 11, 4129–4152, https://doi.org/10.5194/amt-11-4129-2018, 2018.

Tackett, J. L., Kar, J., Vaughan, M. A., Getzewich, B. J., Kim, M., Omar, A. H., Magill, B. E., Pitts, M. C., and Winker, D. M.: The CALIPSO version 4 . 5 stratospheric aerosol subtyping algorithm, 1–42, 2022.

Tackett, J. L., Kar, J., Vaughan, M. A., Getzewich, B. J., Kim, M., Vernier, J., Omar, A. H., Magill, B. E., Pitts, M. C., and Winker, D. M.: The CALIPSO version 4 . 5 stratospheric aerosol subtyping algorithm, 745–768, 2023.

Taylor, I. A., Grainger, R. G., Prata, A. T., Proud, S. R., and Mather, T. A.: A satellite chronology of plumes from the April 2021 eruption of La Soufrière , St Vincent, 15209–15234, 2023.

Tencé, F., Jumelet, J., Bekki, S., Khaykin, S., Sarkissian, A., and Keckhut, P.: Australian Black Summer Smoke Observed by Lidar at the French Antarctic Station Dumont d'Urville, J. Geophys. Res. Atmos., 127, 1–16, https://doi.org/10.1029/2021jd035349, 2022.

Tesche, M., Glantz, P., Johansson, C., Norman, M., Hiebsch, A., Ansmann, A., Althausen, D., Engelmann, R., and Seifert, P.: Volcanic ash over Scandinavia originating from the Grímsvötn eruptions in May 2011, 117, 1–14, https://doi.org/10.1029/2011JD017090, 2012.

Thomason, L. W., Ernest, N., Millán, L., Rieger, L., Bourassa, A., Vernier, J. P., Manney, G., Luo, B., Arfeuille, F., and Peter, T.: A global space-based stratospheric aerosol climatology: 1979-2016, Earth Syst. Sci. Data, 10, 469–492, https://doi.org/10.5194/essd-10-469-2018, 2018.

Toohey, M., Jia, Y., Khanal, S., and Tegtmeier, S.: Stratospheric residence time and the lifetime of volcanic stratospheric aerosols, 3821–3839, 2025.

Torres, O., Bhartia, P. K., Taha, G., Jethva, H., Das, S., Colarco, P., Krotkov, N., Omar, A., and Ahn, C.: Stratospheric Injection of Massive Smoke Plume From Canadian Boreal Fires in 2017 as Seen by DSCOVR-EPIC, CALIOP, and OMPS-LP Observations, J. Geophys. Res. Atmos., 125, 1–25, https://doi.org/10.1029/2020JD032579, 2020.

Trickl, T. and Giehl, H.: 35 yr of stratospheric aerosol measurements at Garmisch-Partenkirchen : from Fuego to Eyjafjallaj ¨ okull , and beyond, 5205–5225, https://doi.org/10.5194/acp-13-5205-2013, 2013.

Trickl, T., Vogelmann, H., Fromm, M. D., Jäger, H., Perfahl, M., and Steinbrecht, W.: Measurement report: Violent biomass burning and volcanic eruptions - a new period of elevated stratospheric aerosol over central Europe (2017 to 2023) in a long series of observations, Atmos. Chem. Phys., 24, 1997–2021, https://doi.org/10.5194/acp-24-1997-2024, 2024.

https://doi.org/10.5194/egusphere-2026-2307
Preprint. Discussion started: 8 May 2026

765 Vaughan, G., Wareing, D., and Ricketts, H.: Measurement Report : Lidar measurements of stratospheric aerosol following the 2019 Raikoke and Ulawun volcanic eruptions, 5597–5604, 2021.

Voudouri, K. A., Michailidis, K., Koukouli, M. E., Rémy, S., Inness, A., Taha, G., Peletidou, G., Siomos, N., Balis, D., and Parrington, M.: Investigating a Persistent Stratospheric Aerosol Layer Observed over Southern Europe during 2019, Remote Sens., 15, https://doi.org/10.3390/rs15225394, 2023.

770 Winker, D. M., Vaughan, M. A., Omar, A., Hu, Y., Powell, K. A., Liu, Z., Hunt, W. H., and Young, S. A.: Overview of the CALIPSO mission and CALIOP data processing algorithms, J. Atmos. Ocean. Technol., 26, 2310–2323, https://doi.org/10.1175/2009JTECHA1281.1, 2009.

Winker, D. M., Liu, Z., Omar, A., Tackett, J., and Fairlie, D.: CALIOP observations of the transport of ash from the Eyjafjallajökull volcano in April 2010, 117, 1–12, https://doi.org/10.1029/2011JD016499, 2012.

775 Young, S. A., Vaughan, M. A., Garnier, A., Tackett, J. L., Lambeth, J. D., and Powell, K. A.: Extinction and optical depth retrievals for CALIPSO's Version 4 data release, Atmos. Meas. Tech., 11, 5701–5727, https://doi.org/10.5194/amt-11-5701-2018, 2018.

Yu, P., Davis, S. M., Toon, O. B., Portmann, R. W., Bardeen, C. G., Barnes, J. E., Telg, H., Maloney, C., and Rosenlof, K. H.: Persistent Stratospheric Warming Due to 2019–2020 Australian Wildfire Smoke, Geophys. Res. Lett., 48,
780 https://doi.org/10.1029/2021GL092609, 2021.

Zerefos, C. S., Eleftheratos, K., Kapsomenakis, J., Solomos, S., Inness, A., Balis, D., Redondas, A., Eskes, H., Allaart, M., Amiridis, V., Dahlback, A., De Bock, V., Diémoz, H., Engelmann, R., Eriksen, P., Fioletov, V., Gröbner, J., Heikkilä, A., Petropavlovskikh, I., JarosÅawski, J., Josefsson, W., Karppinen, T., Köhler, U., Meleti, C., Repapis, C., Rimmer, J., Savinykh, V., Shirotov, V., Siani, A. M., Smedley, A. R. D., Stanek, M., and Stübi, R.: Detecting volcanic sulfur dioxide
785 plumes in the Northern Hemisphere using the Brewer spectrophotometers, other networks, and satellite observations, Atmos. Chem. Phys., 17, 551–574, https://doi.org/10.5194/acp-17-551-2017, 2017.

Zhong, Q., Veraverbeke, S., Yu, P., Ma, J., and Tao, S.: Stratospheric biomass burning aerosols compensate record-breaking ozone depletion over the Arctic in spring 2020, Nat. Commun., 17, 1993, https://doi.org/10.1038/s41467-026-69728-y, 2026.

Zuev, V. V, Burlakov, V. D., Nevzorov, A. V, Pravdin, V. L., and Savelieva, E. S.: 30-year lidar observations of the
790 stratospheric aerosol layer state over Tomsk (Western Siberia , Russia), 3067–3081, https://doi.org/10.5194/acp-17-3067-2017, 2017.

795